MERENTUTKIMUSLAITOKSEN JULKAISU
HAVSFORSKNINGSINSTITUTETS SKRIFT

N:o 243

ISSN 0025-9985

# STUDIES OF THE WINTER-TIME BOUNDARY LAYER OVER THE BALTIC SEA BASED ON PILOT BALLOON SOUNDINGS

SYLVAIN M. JOFFRE

# INTERCALIBRATION OF METHODS FOR CHLOROPHYLL MEASUREMENTS IN THE BALTIC SEA

U. LARSSON, L. NORLING, S. CARLBERG, S. LÖÖF, A. TOLSTOY, K. von BRÖCKL, V. ELIZARJEVA, W. KAISER, J. LASSIG, I. MÄKINEN and T. MELVASALO

MERENTUTKIMUSLAITOKSEN JULKAISU
HAVSFORSKNINGSINSTITUTETS SKRIFT

N:o 243

# STUDIES OF THE WINTER-TIME BOUNDARY LAYER OVER THE BALTIC SEA BASED ON PILOT BALLOON SOUNDINGS

SYLVAIN M. JOFFRE

# INTERCALIBRATION OF METHODS FOR CHLOROPHYLL MEASUREMENTS IN THE BALTIC SEA

U. LARSSON, L. NORLING, S. CARLBERG, S. LÖÖF, A. TOLSTOY, K. von BRÖCKL, V. ELIZARJEVA, W. KAISER, J. LASSIG, I. MÄKINEN and T. MELVASALO

HELSINKI 1978 HELSINGFORS

CONTENTS



ISSN 0025-9985

Helsinki 1978. Government Printing Centre

Merentutkimuslait. julk./Havsforskningsinst. Skr. No. 243 (1978) 3—62

# STUDIES OF THE WINTER-TIME BOUNDARY LAYER OVER THE BALTIC SEA BASED ON PILOT BALLOON SOUNDINGS

Sylvain M. Joffre

Institute of Marine Research,

P. O. Box 166, SF-00141 Helsinki 14

Abstract

Old pibal sounding data from the years 1930—1936 were analysed to investigate the dependence of wind veering and of the ratio between the surface and the upper wind upon stability and baroclinicity. Baroclinicity was assessed through some assumptions concerning the upper wind shear. The surface stress and drag coefficients were thus computed by the ageostrophic method and the results were compared with those of other studies. Next, similarity theory methodology was applied to the data, using both internal and external parameters. The universal similarity functions A and B were calculated. All the results were in fairly good agreement with those obtained in other studies, within the limits of the large scatter generally occurring in connection with such research.

CONTENTS

LIST OF SYMBOLS

| | |
|---|---|
| $A_h$, $B_h$ | Universal similarity functions for a barotropic diabatic planetary boundary layer. |
| $A_i$, $B_i$ | Same as above but in a baroclinic case. |
| $A_{hi}$, $B_{hi}$ | Same as above but in a baroclinic convective case. |
| $C_d$ | Drag coefficient. |
| $C_g$ | Geostrophic drag coefficient. |
| $C_{10}$ | Drag coefficient referred at $z = 10$ m. |
| $D_u$, $D_v$ | Velocity-defect functions between the surface and upper winds relatively to external parameters. |
| $f$ | Coriolis parameter. |
| $g$ | Acceleration due to gravity. |
| $G_o$ | Modulus of the surface geostrophic wind. |
| h | Height of the boundary layer. |
| $\tilde{h}$ | Dimensionless external height ($= hf/V_h$). |
| $H_i$ | Height of zero-stress for boundary layer integration. |
| $K_m$ | Eddy diffusivity coefficient. |
| $L_*$ | Monin-Obukhov length scale ($= -u_*^3/g\beta\kappa Q_o$). |
| $m$, $M_o$, $M_1$ | Constants depending on stability. |
| $N$ | Number of observations. |
| $Q_o$ | Surface heat flux. |
| $r$ | Correlation coefficient. |
| $R$ | Wind velocity ratio ($= V_z/V_z$). |
| $R_h$ | Wind velocity ratio at the top of the boundary layer. |
| $Ri$ | Richardson number. |
| $Ri_z$ | Surface Richardson number. |
| $Ri_z$ | Richardson number centred at $z$. |
| $Ro$ | Rossby number. |
| $S$ | External stability parameter. |
| $S_o$ | Geostrophic shear modulus. |
| $S_u$, $S_v$ | Geostrophic shear components. |
| $S_x$, $S_y$ | Dimensionless geostrophic shear components. |
| $T_a$ | Air temperature. |
| $T_w$ | Sea surface temperature. |
| $u_*$ | Friction velocity. |
| $u$, $v$ | Actual wind components. |
| $U_g$, $V_g$ | Geostrophic wind components. |
| $U_{go}$, $V_{go}$ | Surface geostrophic wind components. |
| $U_{gi}$, $V_{gi}$ | Actual or geostrophic wind at $z = H_i$. |
| $U_{gh}$, $V_{gh}$ | Geostrophic wind components at the top of the boundary layer. |
| $V$ | Wind velocity. |
| $V_z$ | Surface wind velocity. |
| $V_h$ | Wind velocity at the top of the boundary layer. |
| $V_T$ | Thermal wind vector. |
| $z$ | Vertical coordinate. |
| $z_z$ | Height of anemometer level. |
| $z_t$ | Height of air temperature measurement. |
| $z_o$ | Roughness length. |
| $Z^*$ | Height of maximum lateral stress component. |
| $\alpha_z$ | Surface wind direction. |

LIST OF SYMBOLS (cont.)

| | |
|---|---|
| $\alpha_o$ | Surface cross-isobar angle. |
| $\alpha_T$ | Thermal wind direction. |
| $\beta$ | Coefficient of thermal expansion. |
| $\beta_o$ | Angle between the surface geostrophic wind and the thermal wind. |
| $\Delta\alpha$ | Wind veering. |
| $\Delta\alpha_h$ | Wind veering between the surface and the top of the boundary layer. |
| $\Delta\Theta$ | Potential temperature difference between the top and the bottom of the boundary layer. |
| $\zeta$ | Coefficient of surface elevation. |
| $\zeta_h$ | Dimensionless internal stability parameter ($= h/L_*$). |
| $\Theta$ | Potential temperature. |
| K | von Kármán constant. |
| $\mu h$ | Dimensionless internal dynamical parameter ($= hf/u_*$). |
| $\rho$ | Air density ($= 1.2 \times 10^{-3}$ g/cm$^3$). |
| $\tau_o$ | Surface stress. |
| $\tau_{xz}$, $\tau_{yz}$ | Shearing stress components. |
| $\psi$ | Angle measured clockwise from the direction of the wind at $z = 500$ m to the direction of the thermal wind. |
| $\overline{(\ )}$ | Mean quantity. |

## 1. INTRODUCTION

The Gulf of Bothnia is generally ice-covered from January to May. In March, when the ice situation is most severe, the thickness of the ice ranges between 50 and 70 cm. It is important for the Finnish economy that the northern harbours are kept open to trade the whole year round. For this purpose, an ice forecast model has been developed at the Institute of Marine Research, Helsinki (Valli & Leppäranta 1975), which gives 30-hour forecasts for ice drift, ice concentration, ice thickness and ridging intensity.

The equation for ice motion can be written (Campbell 1965):

$$\rho_i \, h_i \, \frac{dV_i}{dt} = \tau_a + \tau_w + C + G + R$$

in which $\rho_i$ is ice density, $h_i$ ice thickness, $V_i$ the ice velocity vector, $\tau_a$ the wind stress acting on the upper surface of the ice, $\tau_w$ the water stress on the lower surface of the ice, $C$ is the Coriolis force due to the earth's rotation, $G$ the surface gradient current due to tilting of the water surface and $R$ the internal stresses between ice floes.

The main term in the above equation is the wind stress term $\tau_a$, which represents a tangential force per unit horizontal area. Therefore its parameterization is very important and is the starting-point of this study.

This wind stress term depends on the roughness of the ice surface, on the shape of the vertical wind profile above the ice surface, which, in its turn, depends on the relation between the wind close to the surface and the wind at upper levels, and on the thermal stability of the atmosphere. Thus, the parameterization of $\tau_a$ requires the investigation of various situations, in order to isolate the influence of these diverse factors. Unfortunately, suitable data, including detailed information on the prevailing environmental conditions, are very rare. However, a set of data was found consisting of old pilot balloon soundings carried out on a small island in the Northern Baltic, and these were processed and analysed, in order to obtain some indications about the dependences and interdependences between the parameters mentioned above (and also of the influence of an often neglected but always present term, the baroclinicity).

With a view to reducing the scatter in the relationships between the dependent and independent variables, combinations of the latter were used in the framework of the so-called similarity theory. This has proved to be a powerful tool in recent years and was applied to the present data in order to estimate its suitability for routine use.

The physical problem involved in the ice-drift phenomenon is a concrete example of air-sea interaction, where the ice cover itself acts as a link between the two elements. This study should be considered a first step in the task of wind stress parameterization.

## 2. THE DATA

Nowadays, radiosonde balloons rise higher and faster than in the past, providing, at most, one or two measurements from the planetary boundary layer. However, this layer, say the lowest kilometre, is characterized by many phenomena of great importance in the basic exchange between the earth's surface and the atmosphere, so that boundary layer data are greatly needed. In recent times, a few extensive boundary layer projects have been organized to collect adequate data for research studies (e.g. Lettau & Davidson 1958, Clarke et al. 1971, Kaimal et al. 1976).

Earlier data also exist, since before the Second World War many routine or special soundings were carried out with pilot balloons or kites. Although these data have some deficiencies (e.g. lack of temperature profiles or surface layer data), they cannot be neglected, since they give extra information on the complex and much too little known variability of the atmospheric boundary layer.

An earlier series of pilot balloon soundings seemed suitable for the present study. They had been performed between June 1929 and June 1936 on the island of Utö, located about 80 km southwest of continental Finland ($\varphi = 59°47'$N, $\lambda = 21°22'$E). The situation of this island on the outskirts of the Åland Archipelago (cf. fig. 1) favours investigations on the marine atmospheric boundary layer, especially for winds from the southern sector (90°, 270°). On the other hand, winds blowing

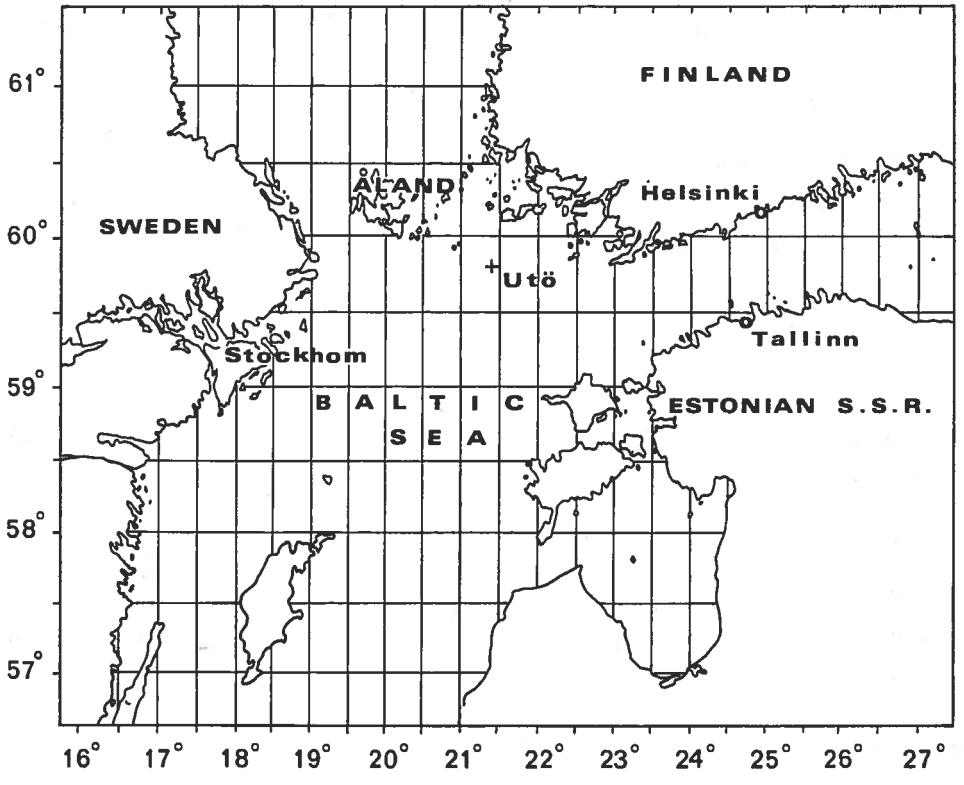


Fig. 1. The study area.

from the north may be expected to be affected firstly by the land-sea transition and secondly by the great number of islands, which will act on the mean flow like large randomly distributed roughness elements.

The material data consist of optically performed pilot sounding measurements (speed of ascent assumed constant). The raw data (inclination and azimuth of the balloon) had already been processed and values were thus available for the wind velocity and wind direction at intervals of 100 m up to 1000 m and intervals of 500 m above that height. Surface wind values had been estimated for a height $z_0 = 15$ m by the staff of the Pilot station. This height will be called henceforth the anemometer height. The fact that the surface wind is estimated is obviously a weakness of these data. The soundings were performed nearly every day and sometimes several times a day (mostly twice but also three, four and even five times).

Since this study deals with the boundary layer structure over sea-ice, attention was restricted to the winter profiles. A survey of the ice reports made at Utö on the basis of visual observations showed that in 1931—1933 and 1936 an ice cover occurred only during some periods in February and March. This is due to the southern location of Utö. For the sake of comparison, and also in order to increase the number of relevant profiles, it was decided to study also the profiles for the ice-free periods occurring during February and March in those years and also the profiles for the ice-free winters of 1930, 1934 and 1935.

Another factor limiting the amount of available data was the optical method of sounding, owing to which a great number of balloons were lost when they rose into clouds or in the direction of the sun. Homogeneous data on the layer showing the strongest wind shear were obtained by selecting the soundings that reached at least 500 m. The wind shear of the upper free flow, which is related to the baroclinicity, was studied by processing all the suitable profiles up to 2000 m. Since the observations were carried out at 500—m intervals above the first kilometre, the balloon often disappeared or burst out between two reference levels (i.e. 1 and 1.5 km or 1.5 and 2 km); in these cases, the balloon's position had been taken just before its disappearance (e.g. at $z = 1300$ m or 1800 m). To avoid the loss of these observations, it was decided to interpolate the profiles at 100—m intervals between 1 and 2 km.

Finally, a total of 250 profiles reaching at least 500 m was available, including 57 profiles for sea-ice situations. Naturally, the number of profiles decreases with increasing $z$, as is shown in Table 1:

TABLE 1. Number of observations at each level.

| Heights (m) | Open water situations | Sea-ice situations | All data | Percentage |
|---|---|---|---|---|
| 0—500 | 193 | 57 | 250 | 100 |
| 600 | 170 | 55 | 225 | 90 |
| 700 | 168 | 53 | 221 | 88 |
| 800 | 159 | 51 | 210 | 84 |
| 900 | 153 | 48 | 201 | 80 |
| 1 000 | 153 | 48 | 201 | 80 |
| 1 100 | 133 | 45 | 178 | 71 |
| 1 200 | 123 | 45 | 168 | 67 |
| 1 300 | 116 | 42 | 158 | 63 |
| 1 400 | 106 | 38 | 144 | 58 |
| 1 500 | 105 | 38 | 143 | 57 |
| 1 600 | 90 | 32 | 122 | 49 |
| 1 700 | 90 | 32 | 122 | 49 |
| 1 800 | 80 | 31 | 111 | 44 |
| 1 900 | 78 | 29 | 107 | 43 |
| 2 000 | 76 | 27 | 103 | 41 |

The time of sounding was most often 9.00, less frequently 15.00 and occasionally 12.00 or 18.00. Table 2 shows the sounding distribution according to the time of day.

TABLE 2. Frequency distribution of observations according to time of day. In each cell the upper figure is the number of observations and the lower figure the percentage.

| | 6 h | 9 h | 12 h | 15 h | 18 h | Total |
|---|---|---|---|---|---|---|
| Sea-ice | 1<br>2 % | 26<br>46 % | 6<br>10 % | 17<br>30 % | 7<br>12 % | 57<br>23 % |
| Open water | —<br>— | 131<br>68 % | 15<br>8 % | 35<br>18 % | 12<br>6 % | 193<br>77 % |
| All observations | 1<br>1/2 % | 157<br>63 % | 21<br>8 % | 52<br>21 % | 19<br>8 % | 250<br>100 % |

Information on the temperature distribution was available at only two levels: i) at $z_t = 2$ m, where the temperature was taken 3 times a day at the station of Utö, and ii) at the sea surface, where the water temperature $T_w$ was taken approximately half a nautical mile west of Utö, about every two weeks. The latter values may be assumed to represent the temperature of the underlying water surface for only a limited area around Utö, since the sea surface temperature has a strong gradient on the southern side of the archipelago (cf. Fig. 2). However, this gradient is stronger at the beginning of the period studied (Fig. 2a for February) and has weakened by the end of March (Fig. 2b), owing to the overall cooling of the Baltic waters towards freezing point. In mild winters (free of sea-ice) a strong temperature gradient exists in the sea surface at the outher edge of the Åland Archipelago, whereas in cold winters this gradient is practically absent, owing to vigorous mixing of the water

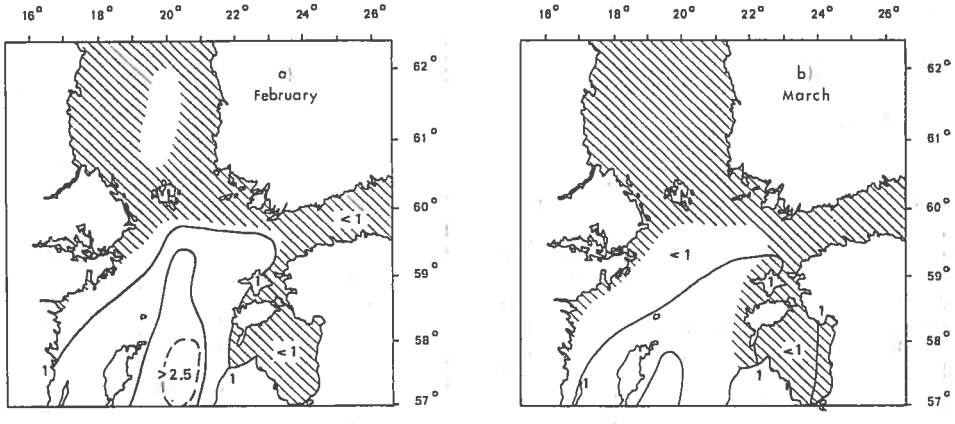


Fig. 2. Average sea surface temperature distribution in the Baltic (1902—1956). The cross-hatched area represents the mean ice cover extent. (After Lenz 1971).

at a temperature close to zero, which in turn results in an extension of the ice cover. Thus, not only the inhomogeneity of the surface topography (cf. Fig. 1), but also the existence of thermal inhomogeneity may influence the development of a new internal equilibrium layer as the air flows over new surface boundary conditions. Thermal inhomogeneity also exists on the northern side of the study area, since the coastal regions of continental Finland show a very strong temperature gradient in wintertime.

## 3. ASSESSMENT OF STABILITY

As the structure of the turbulent atmospheric boundary layer depends greatly on its thermal stability, this stability must be parameterized and assessed, in order to take into account its effect on the profiles. This can be done if either the Monin-Obukhov length or a Richardson number is known. As the data provide no information on the fluxes of momentum and heat, the relevant parameter is the gradient Richardson number defined by

$$\mathrm{Ri} = g\beta \frac{(\partial \overline{\Theta}/\partial z)}{(\partial \overline{V}/\partial z)^2} \tag{1}$$

where g is the acceleration of gravity, $\beta = 1/T_o$ is the inverse of the mean absolute air temperature of the bottom layer, $\overline{\Theta}$ is the mean potential air temperature and $\overline{V}$ the mean wind velocity. The vertical temperature gradient may be approximated with the air-sea temperature difference ($T_a$—$T_w$). As to the velocity gradient, the relevant levels are the anemometer level ($z_s = 15$ m) and the surface, where $V$ vanishes. Writing the derivatives in a discrete form, we obtain a kind of bulk Richardson number, whose expression is:

$$\mathrm{Ri_S} = g\beta \frac{(\mathrm{Ta} - \mathrm{Tw})/z_t}{(V_S/z_S)^2} \tag{2}$$

where $V_s$ is the surface wind velocity. Substituting the values for the constant parameters g, $z_s$ and $z_t$, yields:

$$Ri_s = \frac{1102.5}{T_a} \frac{(T_a - T_w)}{V_s^2} \tag{3}$$

But, this formula is valid only for open water cases, when $T_w$ actually represents the surface temperature. In the case of an ice-covered sea, the surface temperature remains undetermined because, although the temperature of the water just under the ice keeps close to freezing point, the ice surface temperature is strongly depen-

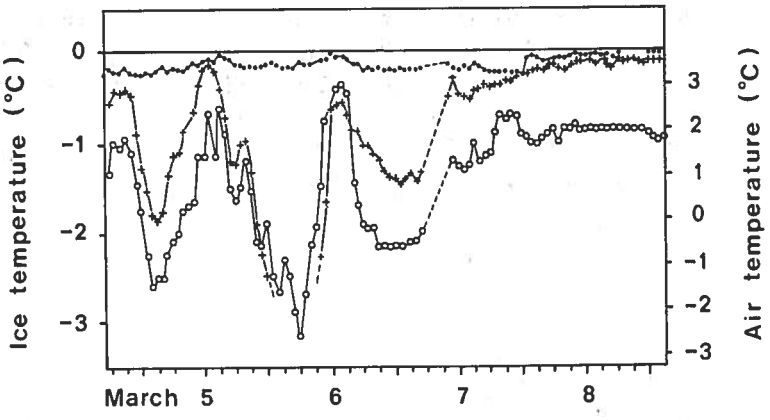


Fig. 3. Air and sea-ice temperature close to Umeå in Northern Sweden (63° 51'N 20°16'E) in March 1975. $T_a$ (open circles) is recorded at $z = 1.5$ m, the crosses are for the ice surface and the full circles for the ice bottom temperature. (After Tabata 1975).

dent on solar radiation, air temperature and the physical and mechanical properties of the ice itself (Zubov 1943), e.g. density, salinity, amount of snow, thermal conductivity, air bubbles within the ice. Thus, the ice surface temperature has a marked daily cycle (Weeks & Lee 1958), cf. Fig. 3.

In consequence, it is impossible to determine $(T_a—T_w)$ in sea-ice conditions and hence $Ri_s$ and the stability conditions are then unknown. Weller (1968), who observed the air stratification over sea ice along the coast of Antarctica ($\varphi = 67°34'$S, $\lambda = 62°53'$E), showed that it was mostly neutral and near-neutral, with a Richardson number $Ri$ centred at $z = 2$ m within the range (—0.05, 0.05) in 80 % of the observations. However, from Fig. 3, it follows that in general we have slight instability when air temperature is below zero and slight stability when it is above. The median value of air temperature in the present 57 runs with sea-ice conditions is —4.4°C, which would give a stability classification of slightly unstable. But this is only an indication.

Next, we report in Fig. 4 the frequency distribution of the Utö data according to the Richardson number $Ri_s$ and the time of day. Only the data for 9 h and 15 h are considered as they include nearly all the observations (68 % and 18 %, respectively, cf. Table 2). One can notice that, in the morning, the distribution is concentrated in the slightly unstable range, whereas in the afternoon it has shifted somewhat towards the stable range. This effect is naturally due to the increase of air temperature $T_a$, which raises the value of $Ri_s$ ($T_w$ remaining the same). The increase of $V_s$ during the course of the day limits the increase of $Ri_s$, which explains the similarity between the two diagrams.

However, these diagrams do not tell the whole truth, because all the observations are included, without reference to, for example, wind direction. Now, owing

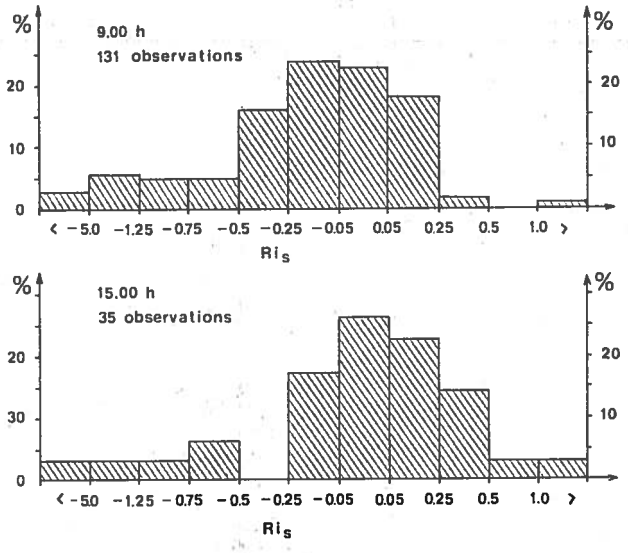


Fig. 4. Frequency distribution of observations according to stability in open-sea situations. The scale of the abscissa it not continuous.

to the geographical configuration of the study area, the features of the boundary layer in Utö may be expected to be strongly dependent on wind direction. This dependence is evident in Fig. 5, which shows the relation between the surface wind direction $\alpha_s$ and the stability parameter $Ri_s$. A clear dependence of $Ri_s$ on $\alpha_s$ appears with the stable cases in the range (120°, 300°) and the unstable cases in the range (0°, 120°) and (300°, 360°). The runs indicated by a triangle in the figure show a »peculiar profile», i.e. a strong turning of the wind ($\geq 90°$) or a strong decrease of the wind with height ($V_s/V_z \geq 2.0$). It is interesting to note that these runs with a peculiar behaviour are located in the wrong domain of stability if the above-mentioned dependence of $Ri_s$ on $\alpha_s$ is correct. These 8 runs (the eighth one is in ice situation) will be eliminated from all the following calculations. Then, stability varies as a sine-like function of wind direction, with its minimum at $\alpha_s \approx 30°$ and its maximum at $\alpha_s \approx 270°$.

The dependence of stability on wind direction was examined in relation to time. No significant difference is apparent between the distributions for February and March, except perhaps a slight shift towards more stable Richardson numbers. This is due to the higher temperature $T_s$ in March. No difference was observable in the distribution of the experimental data with respect to the time of day (9h, 12h, 15h and 18h), probably because the intensity of the diurnal cycle is still weak at this time of the year. Nor did the dependence on wind direction show any difference between winters with ice (1931—1933 and 1936) and warmer winters without ice

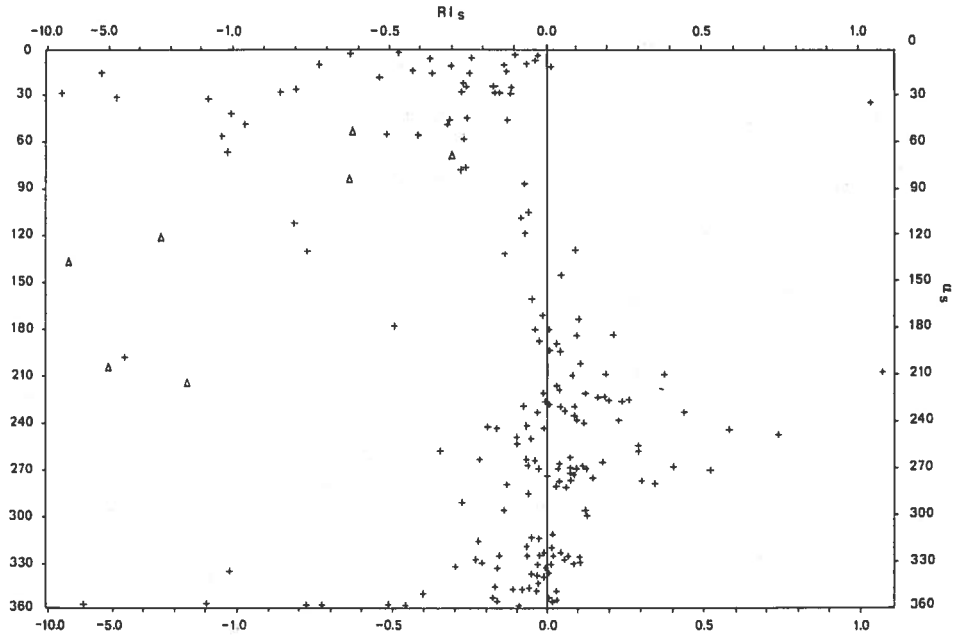


Fig. 5. Dependence of stability on wind direction $\alpha_s$ in open water situations. The triangles ($\Delta$) indicate »peculiar» runs, to be deleted in average computations. The scale of the abscissa is not continuous.

(1930, 1934 and 1935). In consequence, it is possible to deal with the whole set of data regardless of the year, moth or hour of observation. This is an advantage since it saves having to divide the small amount of profiles into even smaller groups.

Geographically, the variation of stability with wind direction means that the stable runs correspond to winds blowing over the sea and the unstable runs to winds coming from cold continental Finland or the Åland Archipelago. Frontal activity is frequent at the latitude of Utö and the discharge of cold northerly winds behind the cyclone results in unstable thermal conditions over the sea.

The stability parameter is useful for classifying the wind profiles, but it must be kept in mind that its value does not always correspond exactly to the true situation, since $T_w$ represents the sea surface temperature only within the immediate vicinity of the island, while $T_a$, which should preferably have been recorded over the waters surrounding Utö, was obtained on land and may be affected by various local factors (radiation, ventilation, refraction, etc. .). The resultant errors in the difference ($T_a$—$T_w$) may be sufficiently great to shift many points in the near-neutral range of stability into a different stability class.

The data were divided into groups according to stability; in order to avoid too small and less representative groups, it was decided to restrict their number to three:

— open water situations with $Ri_s \leq 0$, i.e. unstable cases (124 runs, 49.6 %),
— open water situations with $Ri_s > 0$, i.e. stable cases (69 runs, 27.6 %),
— sea ice situations with $Ri_s$ undefined (57 runs, 22.8 %).

The third group is intermediate between the two other ones, alternatively presenting features of a stable or unstable stratification. This is due to the fact that it contains runs of both types of stratification, which cannot be distinguished on the basis of the available thermal condition data. For the sake of brevity, we shall call these three groups unstable, stable and ice, respectively.

## 4. LOCAL WIND CLIMATOLOGY OF THE TWO LOWEST KILOMETRES OF THE ATMOSPHERE AT UTÖ

### 4.1. GENERAL

The first step in such an investigation is to study the frequency of occurrence of the wind directions and wind velocity. Fig. 6 shows a wind rose for surface winds based on the present set of data. Each branch of the 8-branch rose represents a 45° direction range (338°—22°; 23°—67°; 68°—112°; 113°— 157°; 158°—202°; 203°—247°; 248°—292°; 293°— 337°), its length being proportional to the frequency of winds in this range. This rose differs clearly from the real climatological rose given by Venho (1963) for the period 1931—1960 (cf. Fig. 7), in which the percentage occurrence for each direction range, is almost the same, except for slight maxima for Southwesterlies and Southeasterlies. The present 250 runs show a very irregular distribution, with a marked maximum for Northerlies followed by Southwesterlies, Westerlies and Northwesterlies. Moreover, a complete quadrant (Easterlies, Southeasterlies and Southerlies) has a very low frequency. This departure from the long-term climatological distribution shows that our data are not a representative samble of the general conditions in Utö. Why do north winds predominate in our sample ? One explanation could be a sea-land breeze effect due to the presence of colder land north of the sea area. But no such effect has ever been observed in this region, so a possibly more convinving explanation is that the soundings were made only in favourable observation conditions. In this respect, cloudless conditions would occur during the cold advection following frontal activity already mentioned in the discussion of stability and wind direction.

The evolution of the wind rose with height might be expected to show a general clockwise rotation of the characteristic features of the data rose, but this is not clearly seen in the wind roses for 500 m (Fig. 8) and 1 000 m. In effect, although the Southerlies, Southwesterlies and Westerlies turn clockwise, the Northeasterlies and Northerlies seem to rotate counter-clockwise (this effect is still more apparent with a 12-branch rose). If the surface values are reliable, this means that there is

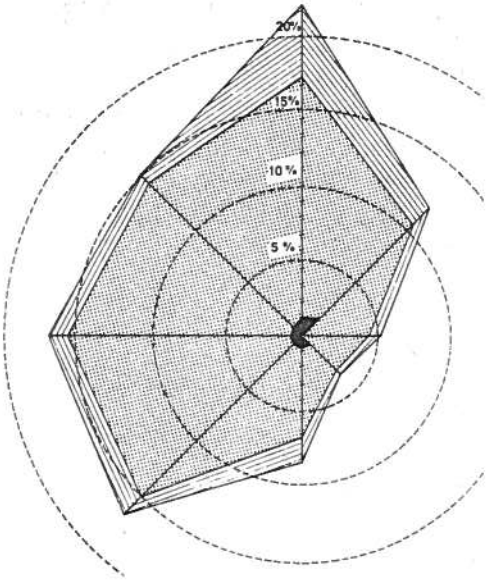


Fig. 6. Surface wind rose for the Utö data (250 observations). The concentric dashed circles indicate the frequency of occurrence.

— weak winds: black area $V \leq 3.3$ m/s.
— moderate winds: dotted area $3.4 \leq V \leq 11.0$ m/s
— strong winds: hatched area $V \geq 11.1$ m/s.

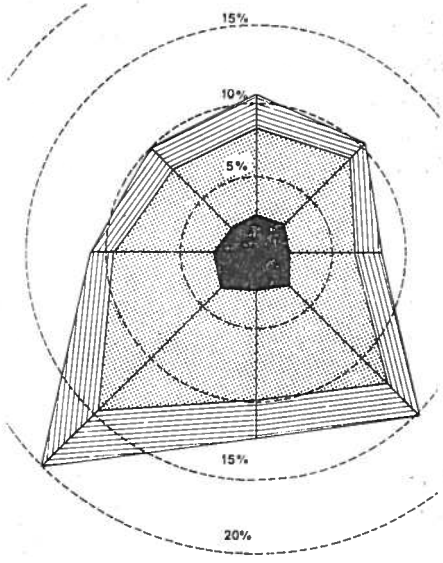


Fig. 7. Climatological wind rose for wintertime (1931—1960) at Utö. For explanation see caption of figure 6. (after Venho 1963).

a thermal wind effect which compensates the frictional veering. By definition, cold advection decreases the veering of the wind (this applies to Northeasterlies and Northerlies) while warm advection increases this veering (this applies to Southerlies, Southwesterlies and Westerlies). Thus these considerations infer a thermal wind from the Northwest sector, and this conclusion is supported by distribution maps of the average upper temperature, such as those in Guterman & Hanevskoi (1963).

As there is no strong difference between the roses at 500 m and 1000 m, the turning of the wind evidently occurs mainly in the first 500 meters of the atmosphere and this may be taken as an estimate of the mean height of the boundary layer.

The wind velocity distribution was also taken into account in the wind roses, the data being divided into three groups: light ($V \leq 3.3$ m/s), moderate ($3.4 \leq V \leq 11.0$ m/s) and strong winds ($V \geq 11.1$ m/s), as was done by Venho (1963). The present data contain a large majority of moderate winds (80 %), while in Venho's

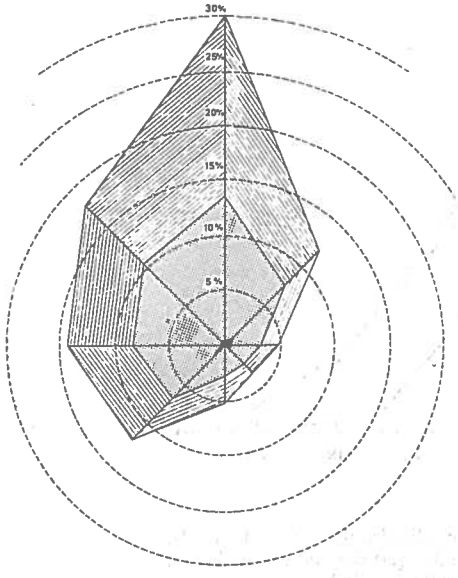


Fig. 8. Wind rose for z = 500 m (250 observations). For explanation see caption of figure 6.

data their proportion is only 56 %. Thus, our data are not biased by the influence of too weak or too strong wind conditions. A better insight into the wind velocity distribution is obtained by subdividing the whole set of data into seven velocity groups ($V < 4$ m/s; $4 \leq V < 8$ m/s; $8 \leq V < 11$ m/s; $11 \leq V < 15$ m/s; $15 \leq V < 19$ m/s; $19 \leq V < 23$ m/s and $V \geq 23$ m/s). The corresponding frequency curves were drawn for surface winds, 500-m-level winds and 1000-m-level winds (Fig. 9). The surface wind curve shows a marked maximum (50 %) for the velocity range 4—8 m/s. This agrees with the value 6.7 m/s given by Kolkki (1969) for the average wind velocity in winter at Utö between 1931 and 1950. No significant difference is apparent between the frequency distributions for the 500-m and 1000-m levels. Thus, this supports our previous choice of the 500-m level as a mean boundary layer height.

In the following, the approach will be to define simple parameters relating conditions close to the surface to conditions in the upper free stream. Obviously, our choice will be limited by the small number of parameters available — wind velocity, wind direction, the estimate of stability conditions close to the water surface and the presence or absence of sea ice.

Two simple descriptive parameters are the velocity ratio $R$ and the wind turning $\Delta\alpha$, defined as:

$$R(z) = V_S/V(z) \tag{4}$$

$$\Delta\alpha(z) = \alpha(z) - \alpha_S \tag{5}$$

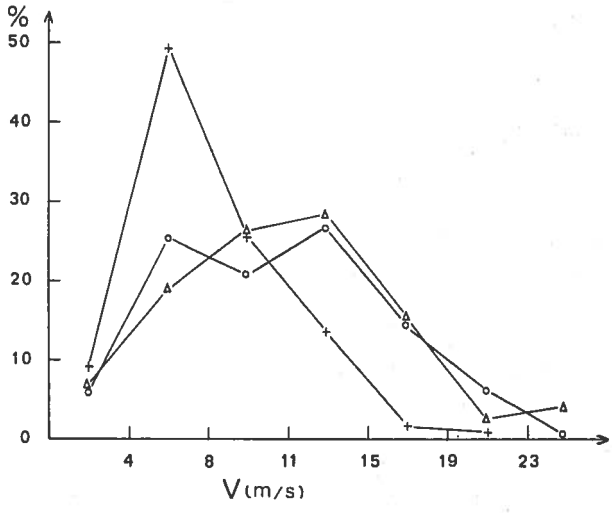


Fig. 9. Wind velocity frequency distribution for 3 levels. Crosses (+) for surface winds, circles (○) for 500-m winds and triangles (△) for 1000-m winds.

If $z$ is chosen to be the height at which geostrophicity is realized, then $R$ relates the surface wind to geostrophic wind and $\Delta\alpha$ represents the turning of the wind within the boundary layer. As variables, one can choose the above-mentioned parameters, i.e. the wind velocity at height $z = h$, which represents the geostrophic forcing of the boundary layer, the wind direction, which includes the dependence on both thermal stability (cf. Fig. 5) and baroclinicity (cf. Figs. 6 and 8), the surface Richardson number $Ri_s$, which estimates stability conditions close to the water surface, and the type of sea surface, which is a measure of both roughness and stability.

The limited amount of data prevents a refined classification, since only larger groups can be representative. Firstly, the whole set of data may be divided into 2 main groups: openwater conditions or sea ice conditions. The former group may then be divided into 2 subgroups according to $Ri_s$: either $Ri_s \leq 0$ (unstable cases) or $Ri_s > 0$ (stable cases); the remaining group of sea-ice conditions may be expected to represent mainly near neutral stability conditions, as the ice surface temperature is very closely related to air temperature. Then, each of these 3 basic groups may be divided into 6 subgroups according to surface wind direction. Some subjectivity has been introduced in the choice of the range of these direction groups, by using geographical origin and the distribution of the observation points of Fig. 5. The groups are:

i) $1° \leq \alpha_s \leq 80°$, winds from continental Finland, very unstable;
ii) $81° \leq \alpha_s \leq 110°$, winds from the Gulf of Finland, unstable;
iii) $111° \leq \alpha_s \leq 170°$, winds from Esthonia, near-neutral;
iv) $171° \leq \alpha_s \leq 240°$, winds from the Baltic Proper, stable;
v) $241° \leq \alpha_s \leq 290°$, winds from Sweden, stable;
vi) $291° \leq \alpha_s \leq 360°$, winds from the Archipelago, unstable.

The stability classification mentioned for each direction group refers only to the mean trend of the said group, but, of course, runs with different stability may occur within the same group. Finally, each of these $3 \times 6$ groups may be divided according to the strength of the geostrophic wind, assumed to be reached at $z = 500$ m. Thus, a weak wind group ($V_{500} \leq 10$ m/s) and a strong wind group ($V_{500} > 10$ m/s) are created.

## 4.2. THE WIND VELOCITY RATIO

Values of $R(z = 500)$ for various arrangements according to $\alpha_s$, $Ri_s$, $V$ (500) and the state of the sea are shown in Table 3, and the variations with the surface wind direction $\alpha_s$ are illustrated in Fig. 10. At first sight there appears to be great variability with a large scatter, and some significance is lost owing to the small amount of observations in certain cells. However, an attempt can be made to explain the values obtained and to compare them with the results of previous research.

The overall mean 0.745 falls between the value 0.7 given by Gordon (1950) for the ratio $V(15)/V(600)$ over the North Atlantic and the value 0.8 obtained by Findlater et al. (1966) for the ratio $V(18)/V(900$ mb) at the ocean weather station I and J. Hasse & Wagner (1971) also obtained values of the ratio $R = V(10)/V_g$ between 0.7 and 0.8 for values of the geostrophic wind $V_g$ within the range 10—20 m/s. As has been noted in all earlier studies, we find that the ratio is generally higher for weak 500-m winds ($V_{500} \leq 10$ m/s). The dependence of R on $\alpha_s$ was also investigated for two other choices of the boundary layer height, namely 300 and 800 m. The former might correspond better to very stable cases and the latter to slight convection conditions. The general trend of the curves does not change basically with h, except in some cases where the amount of data is too small.

An important point is the assessment of thermal stability effects. The overall means show a continuous increase of R from stable open-water conditions (0.679) through ice conditions (0.766) to unstable open-water conditions (0.782). This result is expected (see, e.g., Roll (1965), who quotes values for the ratio $V_s/V_g$ varying from 0.55 to 0.8 when the air-sea temperature difference $T_a - T_w$ varies from +4°C to —8°C), since stable wind profiles show a stronger shear than uns-

TABLE 3. The ratio $R_{500}$ as a function of $\alpha_s$, $Ri_s$, $V_{500}$ and the state of the sea. The figures are mean values with their standard deviations (±) and the number of cases (figures at the right of the solidus).

| SEA | Ris | V500 | $0 \leq \alpha_s \leq 80$ | $81 \leq \alpha_s \leq 109$ | $110 \leq \alpha_s \leq 170$ | $171 \leq \alpha_s \leq 240$ | $241 \leq \alpha_s \leq 290$ | $291 \leq \alpha_s \leq 360$ | $0 \leq \alpha_s \leq 360$ |
|---|---|---|---|---|---|---|---|---|---|
| WATER | >0 | ≤10 | .57±.0 /1 | — | .80±.18/2 | .96±.30/12 | .67±.19/10 | .69±.10/6 | .79±.27/31 |
| | | >10 | .70±.0 /1 | — | — | .60±.13/14 | .55±.13/14 | .62±.14/9 | .59±.13/38 |
| | | ALL | .64±.07/2 | — | .80±.18/2 | .76±.29/26 | .60±.17/24 | .65±.13/15 | .68±.23/69 |
| ICE | ALL | ≤10 | .84±.42/5 | .92±.20/3 | .83±.08/4 | .97±.15/5 | .86±.26/5 | .67±.26/6 | .84±.28/28 |
| | | >10 | .71±.13/6 | .90±.0 /1 | .69±.04/2 | .70±.11/4 | .63±.19/5 | .59±.13/10 | .66±.15/28 |
| | | ALL | .77±.31/11 | .91±.17/4 | .78±.09/6 | .85±.19/9 | .74±.26/10 | .62±.19/16 | .75±.24/56 |
| WATER | ≤0 | ≤10 | .85±.35/22 | 1.21±.0 /1 | .90±.16/5 | 1.41±.49/4 | .84±.18/10 | .76±.20/17 | .87±.33/57 |
| | | >10 | .70±.13/21 | .71±.0 /1 | .76±.11/4 | .69±.18/7 | .64±.25/6 | .70±.17/21 | .70±.16/60 |
| | | ALL | .78±.27/43 | .96±.25/2 | .82±.15/9 | .95±.48/11 | .77±.23/16 | .72±.19/38 | .78±.27/117 |
| ALL | ALL | ≤10 | .84±.36/28 | .99±.21/4 | .84±.14/9 | 1.05±.37/21 | .78±.22/25 | .73±.20/29 | .84±.30/116 |
| | | >10 | .70±.12/28 | .81±.13/2 | .74±.11/5 | .64±.15/25 | .59±.18/25 | .65±.16/40 | .66±.16/126 |
| | | ALL | .77±.28/56 | .93±.20/6 | .80±.14/15 | .83±.34/46 | .68±.22/50 | .68±.18/69 | .74±.26/242 |

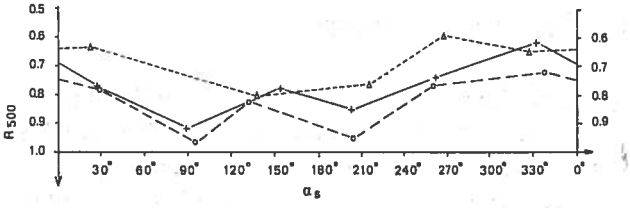


Fig. 10. Dependence of the ratio R (500) on the surface wind direction $\alpha_s$. +———+, sea-ice cases; o— — —o, unstable cases; Δ·····Δ, stable cases.

table ones. As can be seen in Fig. 10, this is true whatever the wind direction, the only exception being the group (291°—360°), where R (ice) < R (stable). The three curves show the same pattern, with smaller values for R in the groups (241°—290°), (291°—360°) and (0°—80°). As these groups represent opposite conditions of stability (241°—290° and 291°—360°) and opposite conditions of surface roughness (241°—290° and 0°—80°), it is probable that the observed trends are due to baroclinicity, which is an ever-present phenomenon, as was pointed out in the discussion of the wind roses.

According to Frost (1948), the ratio of surface to geostrophic wind has the form:

$$V_s/V_g \propto (z_0 V_g)^{-m/(1+2m)} \qquad (6)$$

where $z_0$ is the roughness length and $m$ a stability parameter. According to Frost's (1948) and Charnock's (1955) studies, it appears that $z_0$ is proportional to $V_g$, so that expression (6) reduces to:

$$V_S/V_g = A(V_g)^{-m} \tag{7}$$

where $A$ is a proportionality coefficient. Expression (7) is illustrated in Fig. 11, where the empirical points are the mean values of the groups in Table 3. From these data, nonlinear regression curves can be obtained for the three different samples corresponding to ice, stable and unstable cases. The numerical values are shown in Table 4.

TABLE 4. Regression values of the coefficient $m$ and $A$ for three different samples of data. $r$ is the correlation coefficient.

| | $Ri_g \leq 0$ | Ice | $Ri_g > 0$ |
|---|---|---|---|
| m | 0.309 | 0.323 | 0.398 |
| A | 1.588 | 1.534 | 1.712 |
| r | —0.86 | —0.72 | —0.79 |

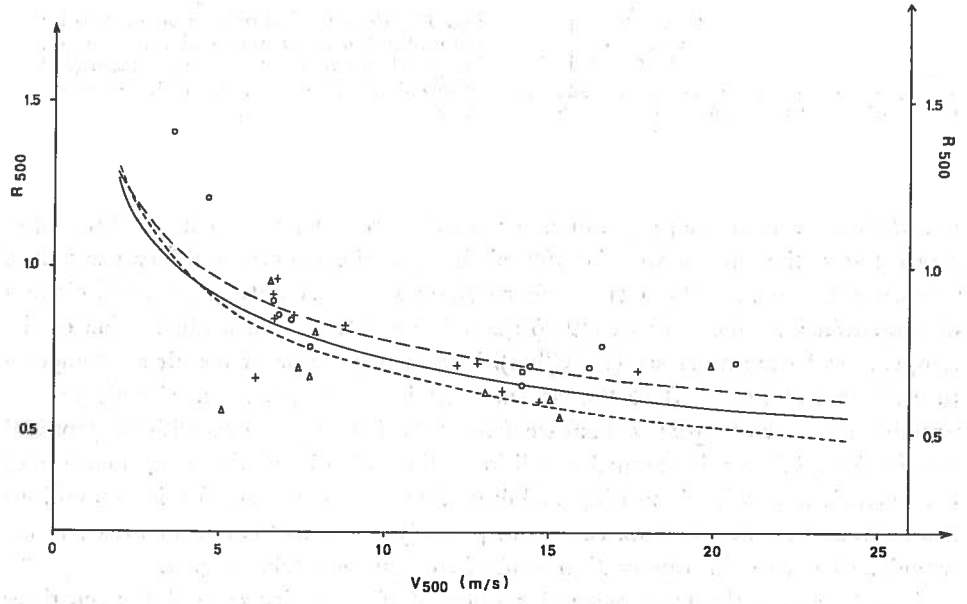


Fig. 11. Dependence of the ratio $R_{500}$ on the wind velocity $V_{500}$. The data correspond to the mean values of each different group in Table 3. The curves represent the best regression fit for the three stability stratification. +———+, ice cases; o— — —o, unstable cases; Δ·····Δ, stable cases.

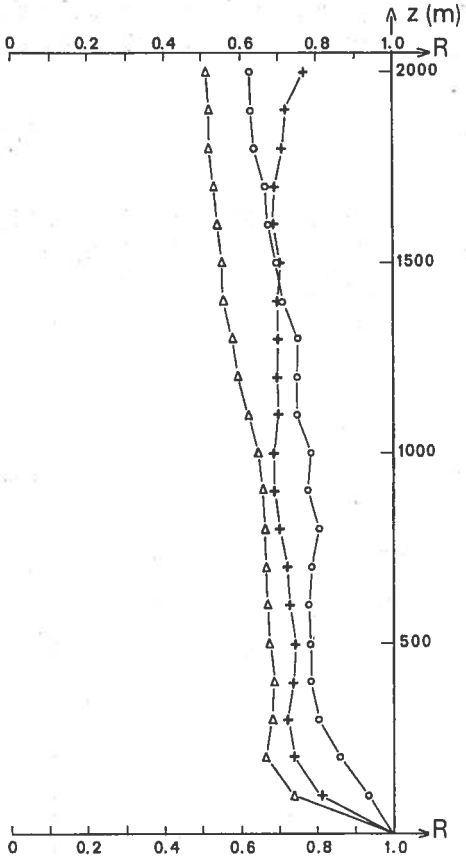


Fig. 12. Mean vertical profiles of the velocity ratio R for 3 different stratifications. +——+, ice (56 observations) ○——○, unstable (117 observations) △——△, stable (69 observations)

It is difficult to compare these values for $m$ with those of Frost, as he used the lapse rate between the surface and the 900-mb level as the relevant stability parameter, whereas the present Richardson number describes stability only in the close vicinity of the surface. Findlater et al. (1966) quoted $m = 0.2$ for the median value of the temperature lapse rate at sea (7.3°C/km). The median value of the air-sea temperature differences ($T_a$—$T_w$) of the present data is —2.2°C, i.e. also slightly on the unstable side. Frost made $m$ increase from 0.17 for unstable conditions (lapse of 10°C/km) to 0.3 for isothermal conditions; thus we obtain the same increase of the coefficient $m$ with increasing stability. The group of data for ice conditions lies between the two open-sea cases, but possibly closer to the unstable case, which would agree with the observation made in connection with Fig. 3.

Fig. 12 shows the mean vertical profiles of the velocity ratio R for the three different stability classes, including all directions. The profiles are not completely smooth as the number of available data decreases upwards from 500 m. The curves

for the lowest 500 m are, however, rather significant since the amount of observations is constant for the six first levels (including the anemometer level). The height of the friction layer (i.e. the layer where the wind ranges from zero to its free stream value) can be seen to vary, showing a shallower value for the stable case (the minimum of $R$ is still more apparent for the subgroup 171°—240°, which is the most stable). These profiles also support our assumption that the wind has reached geostrophic equilibrium at $z = 500$ m. Another interesting feature is the sloping of all the $R$ profiles above 800 m, which indicates the presence of thermal wind effects. A general trend is a decrease of $R$ with increasing height.

## 4.3 WIND VEERING

The data were classified in the same subgroups as those used in section 4.2, in order to try to explain the variations of the turning of the wind between the surface and

TABLE 5. The turning of the wind $\Delta\alpha_{500}$ (in degrees) as a function of the state of the sea, stability, wind direction and wind velocity at 500 m. For explanation see caption of Table 3.

| SEA | $Ri_s$ | V500 | $0 \leq \alpha_s \leq 80°$ | $\leq 81° \leq \alpha_s 109°$ | $110° \leq \alpha_s \leq 170°$ | $171° \leq \alpha_s \leq 240°$ | $241° \leq \alpha_s \leq 290°$ | $291° \leq \alpha_s \leq 290°$ | $0° \leq \alpha_s \leq 360°$ |
|---|---|---|---|---|---|---|---|---|---|
| WATER | $> 0$ | $\leq 10$ | −32±0 /1 | — | 52±11/2 | 41±21/12 | 41±14/10 | 16±23/6 | 35±25/31 |
| | | $> 10$ | − 5±0 /1 | — | — | 26±21/14 | 40±18/14 | 19±14/9 | 29±21/38 |
| | | ALL | −18±13/2 | — | 52±11/2 | 33±22/26 | 41±16/24 | 18±18/15 | 31±23/69 |
| ICE | ALL | $\leq 10$ | 17±12/5 | 31±6 /3 | 20±14/4 | 12±17/5 | 35±7 /5 | − 1±42/6 | 17±25/28 |
| | | $> 10$ | 8±10/6 | 18±0 /1 | 15±11/2 | 25±14/4 | 26±18/5 | 16±11/10 | 17±14/28 |
| | | ALL | 12±12/11 | 28± 7/4 | 18±14/6 | 17±17/9 | 31±14/10 | 10±28/16 | 17±21/56 |
| WATER | $\leq 0$ | $\leq 10$ | 2±23/22 | −22± 0/1 | − 3±27/3 | 20±12/4 | 15±18/10 | 9±13/17 | 7±21/57 |
| | | $> 10$ | 6±16/21 | 18± 0/1 | 13±14/4 | 16± 7/7 | 4±19/6 | 7±11/21 | 8±14/60 |
| | | ALL | 4±20/43 | − 2±20/2 | 6±22/7 | 18±10/11 | 11±19/16 | 8±12/38 | 8±18/117 |
| ALL | ALL | $\leq 10$ | 4±23/28 | 18±23/4 | 19±28/9 | 30±23/21 | 29±19/25 | 8±25/29 | 17±26/116 |
| | | $> 10$ | 6±15/28 | 18± 0/2 | 14±14/5 | 23±18/25 | 29±23/25 | 12±13/40 | 16±19/126 |
| | | ALL | 5±20/56 | 18±19/6 | 17±23/15 | 26±20/46 | 29±21/50 | 10±19/69 | 17±22/242 |

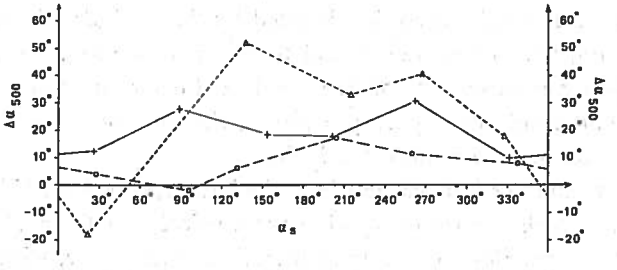


Fig. 13. Dependence of the wind veering $\Delta\alpha$ (500) on the surface wind direction $\alpha_s$. +——+, sea-ice cases; o— — —o, unstable cases; Δ·····Δ, stable cases.

the 500-m level, taken as the top of the boundary layer. The problem of the determination of the turning of the wind is a very important one in general and essential in the case of ice-drift studies.

Values of $\Delta\alpha$ (500) for various classes of surface, stability, wind velocity and wind direction are presented in Table 5, and illustrated in Fig. 13. From these it appears that the veering angle has a great dependence on wind direction and stability but no clear correlation with wind velocity. The angle was sometimes not even smaller with stronger winds, which indicates that baroclinicity probably has a disturbing effect. The overall mean of 16.6° is somewhat higher than the values obtained by Findlater et al. (1966) at ships I and J (7° and 9° respectively) and higher than those reported by Mendenhall (1967) from Johnston Island (4°) and ship *N* (2°), though smaller than his value from Swan Island (21°). The average value for all water situations (16.4°), including all stability conditions, is nearly equal to the ice condition value (17.1°). However, the scatter of the individual veering values is wide and the standard deviation is generally greater than the mean. A not significant part of the observations, from 6 % (stable) to 31 % (unstable), shows backing of the wind at $z = 500$ m (see Table 6).

TABLE 6. Frequency of occurrence of wind backing according to height and stability.

| z | Unstable | Ice | Stable | All |
|---|---|---|---|---|
| 300 m | 24 % | 14 % | 8 % | 17.5 % |
| 500 m | 31 % | 14 % | 6 % | 20.0 % |

These values are in good agreement with Sheppard et al.'s (1952) observation that in 30 % of cases the wind at 300 m was backed on the surface wind (their air-sea temperature difference has a median value of —0.8°C, i.e. slightly unstable).

As expected, the veering angle $\Delta\alpha$ (500) is seen in Fig. 13 to be greatest for stable conditions and smallest for unstable conditions. However, these trends are inverted in the range (0°—80°), where the stable wind shows backing. This direction range corresponds to winds blowing from Finland, i.e. from over a surface that is generally much colder. The cold advection implied by these winds will cause a counterclockwise rotation, which has been found to be as strong as 70° (Hoxit, 1974) and can easily explain our observed value. Our data do not show any clear relation between $\Delta\alpha_{500}$ and wind velocity at $z = 500$ m, the only observable trend is a decrease of the scatter wind increasing velocity.

Fig. 14 shows the vertical distribution of wind veering for stable, unstable and ice situations. As in the figure illustrating the vertical variations of the wind velocity ratio, the three profiles are clearly distinct from each other, with strong veering in the lowest 200 m in stable conditions and a small angle nearly constant with height for unstable situations. Although the overall mean profiles show no trend at upper

levels, the profiles for the specific direction groups show a more or less linear trend above 500 m, this variation being positive or negative according to the group. However, no clear correlation could be found between the signs of the upper trends of $R$ and $\Delta\alpha$ in the same direction groups.

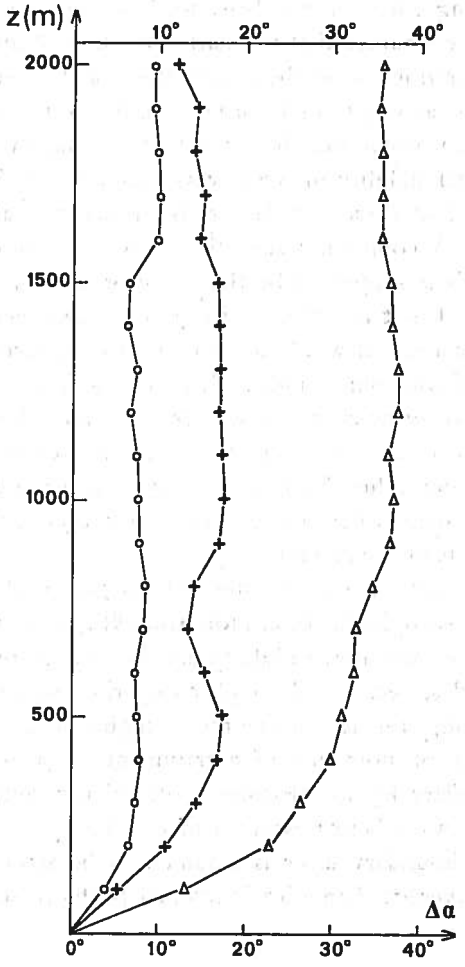


Fig. 14. Mean vertical profiles of the veering angle $\Delta\alpha$ for three different stratifications. +———+, ice (56 runs) o———o, unstable (117 runs) Δ———Δ, stable (69 runs).

# 5. COMPUTATION OF THE PROPERTIES OF BAROCLINIC BOUNDARY LAYERS

## 5.1. ASSUMPTIONS AND THEORY

The parameterization of boundary layer properties, such as the surface stress or the cross-isobaric angle, requires quantitative knowledge of their dependence on the various possible conditions occurring in the nature (wind velocity, thermal stability and baroclinicity). The influence of baroclinicity, in particular, seems to require attention, since on many occasions in the previous sections we have noted its probable disturbing effect on the behaviour of the actual boundary layer.

A major problem encountered at the start is the lack of information on the horizontal temperature distribution in the lowest layer of the atmosphere. We are thus obliged to make some assumptions in order to estimate the degree of baroclinicity. The shape of the wind profile may be assumed to be mainly determined by surface roughness and thermal stability in the lowest kilometre of the atmosphere. Above that height, the effect of these two factors is probably small, and baroclinicity is the dominant factor. A common assumption is that the geostrophic shear is constant with height (this is supported by the shape of the upper part of our profiles, e.g. Fig. 12). This makes it possible to determine the surface geostrophic wind by extrapolating the upper actual wind values down to the surface. The common way of determining the geostrophic wind, which follows from its definition, is to use the surface pressure synoptic charts. However, even nowadays, this method is very hazardous, since a small error in the drawing of the isobars can lead to a major error in the geostrophic wind value. This is even truer with old synoptic charts related to the present set of data, where the observation station network is sparse and the measurements less reliable than now.

Accordingly, we shall assume that the wind is geostrophic at $z = 2000$ m and use the so-called ageostrophic method (Johnson 1962) to estimate the surface wind stress. The level chosen was much higher than the average of 500 m obtained from the actual wind profiles, because, although equilibrium seems to be reached at that height, geostrophic adjustment occurs only at higher levels (especially in unstable conditions, where the phenomenon of entrainment involves large stress values at the top of the boundary layer). Moreover, the thicher layer given by the choice of $H_i = 2000$ m allows a better estimate of $\partial V_g/\partial z$.

As is usual, the boundary layer is assumed to be stationary (this assumption accords better with average than with individual profiles), so that the equations of motion are:

$$\frac{\partial \tau_{xz}}{\partial z} = -\rho f (v - V_g) \tag{8}$$

$$\frac{\partial \tau_{yz}}{\partial z} = \rho f (u - U_g) \tag{9}$$

where $\tau = \tau_{xz}\,\hat{i} + \tau_{yz}\,\hat{j}$ is the wind stress vector, $\rho$ the air density, $f$ the Coriolis parameter, and $(u, v)$ and $(U_g, V_g)$ the longitudinal and lateral components of the actual and geostrophic wind respectively.

With the x-axis oriented along the surface wind (i.e. the wind at anemometer height), we have the following lower boundary conditions:

$$\tau_{xz} = \tau_0 \quad , \quad \tau_{yz} = 0 \qquad \text{at} \quad z = z_0 \tag{10}$$

For the upper boundary condition, both stress components are assumed to vanish at the height $z = H_i$

$$\tau_{xH_i} = \tau_{yH_i} = 0 \tag{11}$$

Then, when equations (8) and (9) are integrated from the surface to the height $H_i$, they become:

$$\tau_0 = \rho f \int_0^{H_i} (v - V_g)\, dz \tag{12}$$

$$0 = \rho f \int_0^{H_i} (u - U_g)\, dz \tag{13}$$

Equation (13) will be an useful constraint for assessing the geostrophic wind profile needed to compute our basic unknown $\tau_0$.

As said before, we assume that the vertical variation of the geostrophic wind is linear, i.e. $U_g = U_{g0} + S_u\, z$ and $V_g = V_{g0} + S_v\, z$, where $U_{g0}$ and $V_{g0}$ are the surface geostrophic wind components, and the slopes of the components are expressed by the constant terms $S_u = \partial U_g / \partial z$ and $S_v = \partial V_g / \partial z$. Replacing these terms in (13), we get:

$$\int_0^{H_i} u\, dz = \int_0^{H_i} U_{g0}\, dz + \int_0^{H_i} S_u\, z\, dz$$

$$\int_0^{H_i} u\, dz = H_i \left(U_{g0} + \tfrac{1}{2} S_u H_i\right)$$

The integral of the left-hand side can be calculated by planimetry or by simple integration on a computer of the profile data, so the unknown is the longitudinal component of the surface geostrophic wind $U_{g0}$. The geostrophic shear $S_u$ is also unknown, but the assumption of linearity gives:

$$S_u = (U_{gi} - U_{g0})/H_i$$

with $U_{gi} = u\ (z = H_i)$. Then we have.

$$U_{g0}=\frac{2}{H_i}\int_0^{H_i} u\,dz - U_{gi} \tag{14}$$

The lowest point of intersection of the linear geostrophic wind profile and the observed u-profile determines a level $Z^*$ at which $\tau_{yz}$ is at a maximum, since $\tau_{yz}$ increases up to this height and then decreases in the interval between $Z^*$ and $H_i$, to a value of zero at $z = H_i$ (Johnson 1962). Integration of equations (8) and (9) from the surface to this height $Z^*$ yields:

$$\tau^*_{xz} - \tau_0 = -\rho f\int_0^{Z^*} (v - V_g)\,dz \tag{15}$$

$$\tau^*_{yz} = \rho f\int_0^{Z^*} (u - U_g)\,dz \tag{16}$$

As both the $u$- and $U_g$-profiles are known, so is the integral on the right-hand side of equation (16). On the other hand, the semi-empirical parameterization of the vertical stress components gives:

$$\tau_{xz} = K_m\frac{\partial u}{\partial z} \quad ; \quad \tau_{yz} = K_m\frac{\partial v}{\partial z}$$

The identity of the eddy diffusivity coefficient $K_m$ in the two components may be justified from tensorial invariance considerations or from the results of a higher-order model of turbulence (Monin 1965). We can then write

$$K_m = \tau_{xz}/(\partial u/\partial z) = \tau_{yz}/(\partial v/\partial z)$$

This equality is also true at $z = Z^*$,

$$K^*_m = \tau^*_{xz}/(\partial u/\partial z)^* = \tau^*_{yz}/(\partial v/\partial z)^* \tag{17}$$

The term $\tau^*_{yz}$ is known from (16), the slopes of the $u$ and $v$ profiles at $z = Z^*$ are determined graphically and then $\tau^*_{xz}$ is obtained from (17).

Besides, substitution of (12) in (15) gives

$$\tau^*_{xz} = \rho f\int_{Z^*}^{H_i} (v - V_g)\,dz \tag{18}$$

With our assumption of a constant thermal wind ($V_g = V_{g0} + S_v z$ and $S_v = \text{const.}$), (18) takes the form

$$\tau^*_{xz} = \rho f\left[\int_{Z^*}^{H_i} v\,dz - V_{g0}(H_i - Z^*) - \tfrac{1}{2}S_v(H_i^2 - Z^{*2})\right] \tag{19}$$

After substitution of (17), (16) and $S_v = (V_{gi} - V_{g0})/H_i$ in (19), we obtain the following expression for the lateral component of the geostrophic wind:

$$V_{g0} = \frac{\int_{Z^*}^{H_i} v\,dz - \frac{V_{gi}}{2H_i}(H_i^2 - Z^{*2}) - \left[\left(\frac{\partial u}{\partial z}\right)^*/\left(\frac{\partial v}{\partial z}\right)^*\right]\int_0^{Z^*}(u - U_g)\,dz}{(H_i - Z^*)\left(1 - \frac{(H_i + Z^*)}{2H_i}\right)} \tag{20}$$

Once $V_{g0}$ is known, the $V_g$-profile is known and so the computation of the surface stress is straightforward, with the aid of (12)

$$\tau_0 = \rho f\left[\int_0^{H_i} v\,dz - H_i\left(V_{g0} + \tfrac{1}{2} S_v H_i\right)\right] \tag{21}$$

From these three quantities other important and interesting quantities can be computed. One of them is the so-called cross-isobar angle $\alpha_0$, which expresses the deviation of the surface wind from the surface geostrophic wind. It is defined as follows:

$$\alpha_0 = \tan^{-1}\left(\frac{V_{g0}}{U_{g0}}\right) \tag{22}$$

In modelling ice drift, the simplest parameterization of the wind stress is through a drag coefficient $C_d$ or a geostrophic drag coefficient $C_g$ in the expressions

$$\tau_0 = \rho\, C_d\, V_s^2 \tag{23}$$

$$\tau_0 = \rho\, C_g\, G_0^2 \tag{24}$$

where $G_0 = (U_{g0}^2 + V_{g0}^2)^{1/2}$. We can then compute $C_d$ and $C_g$ if we know $\tau_0$, the surface wind or the surface geostrophic wind. These coefficients, which basically represent the surface roughness, may also vary with wind velocity itself and with thermal stability, but although abundant empirical data have been compiled for these variations, some disagreement still exists about the results. This may be due to the fact that the field measurements are representative only of the very place where they have been carried out, and moreover it is difficult to compare the conditions of inhomogeneity, nonstationarity and baroclinicity between one place and another.

One of the basic parameters used in the classification of the observation data was a measure of thermal stability consisting of a surface Richardson number $Ri_*$. Lettau (1962) derived an expression for the Richardson number without knowledge of the vertical temperature distribution. This rests on the assumption that vertical heat convection balances horizontal temperature advection, i.e.

$$u\frac{\partial\Theta}{\partial x} + v\frac{\partial\Theta}{\partial y} = \frac{\partial}{\partial z}\left(K_T\frac{\partial\Theta}{\partial z}\right)$$

where $K_T$ is a coefficient of thermal eddy diffusivity. The omission of the time variation of the temperature may be justified when average data are taken, so that the variation is smoothed out. A precise derivation of the expression for the Richardson number centred at a height $z$ can be found in Johnson (1962), here we shall merely consider the final result:

$$Ri_z = \kappa f \frac{(U_{gi}\, V_{g0} - U_{g0}\, V_{gi})}{(\tau_0/\rho)^{3/2}}\, z \qquad (25)$$

where **K** is the Von Karman constant ($\approx 0.4$) and the expression between parenthesis is the advectional term. Computation of the Richardson number given by equation (25) will serve to check the agreement with our defined surface Richardson number. In the computation, we shall take $z = (z_s z_i)^{1/2} \approx 5.5$ m as the level at which $Ri_z$ is centred.

## 5.2. RESULTS OF THE COMPUTATIONS

The computational procedure presented in section 5.1 was applied to 14 selected mean profiles differentiated by stability and surface wind direction. The hodographs of these 14 profiles are shown in Fig. 15 with the computed thermal wind vector. The geostrophic wind vector also represented in these hodographs will be defined in section 7.1. The computed geostrophic wind and the observed wind profiles were in close agreement above 1000 m, thus supporting the assumptions made. Of course, a larger amount of observation data would have smoothed the actual wind profiles and thus improved possibilities for comparison and for the assessment of, for instance, the geostrophic adjustment height.

The results of the computation of the different parameters presented in the previous section are given in Table 7. The cross-isobar angle values $\alpha_0$ show the expected decreasing trend from large values in stable conditions (mean = 27.2°) through ice condition values (slighty stable) with a mean of 20.6° to smaller values in unstable conditions.

The drag coefficient and surface stress values show a large scatter, and in some cases they are very unlikely. On one occasion, the surface stress even takes a negative value, thus indicating a momentum transfer from the sea surface towards the atmosphere. These values will be dealt with in more detail in the next section.

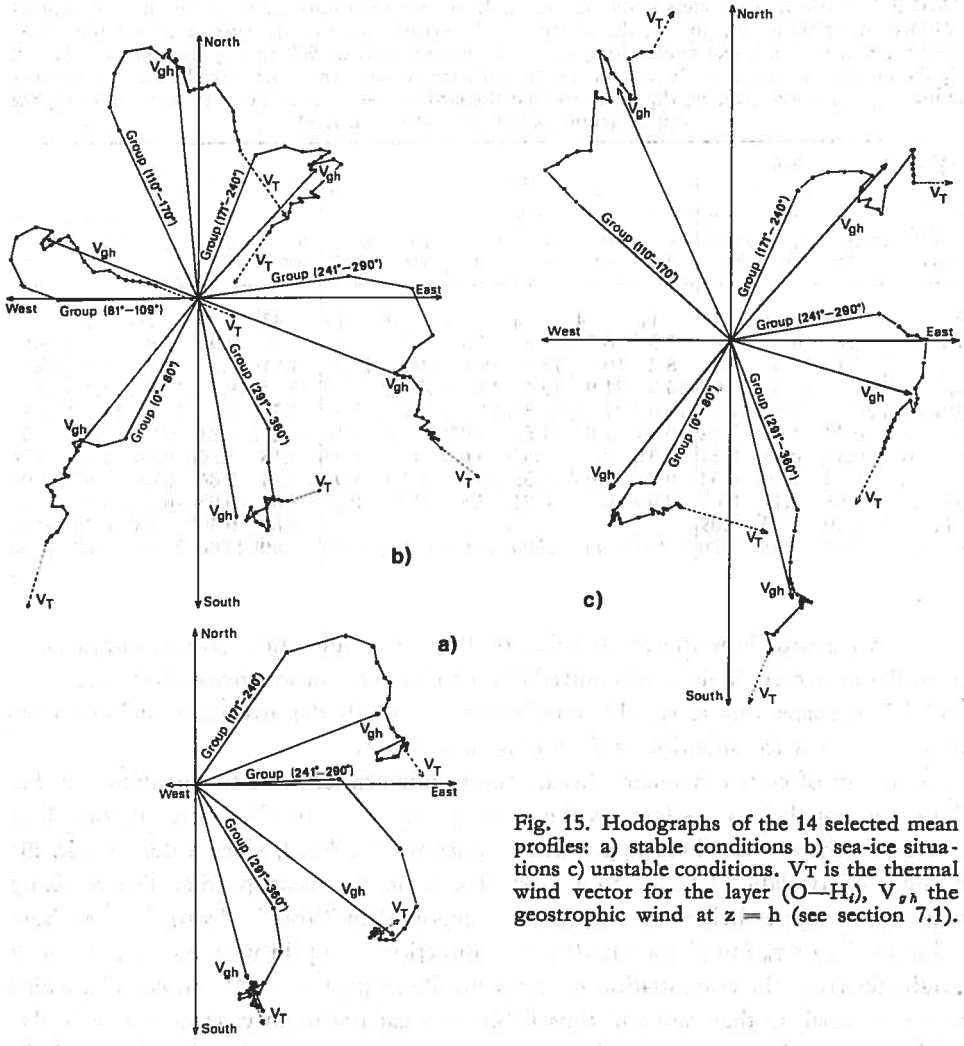


Fig. 15. Hodographs of the 14 selected mean profiles: a) stable conditions b) sea-ice situations c) unstable conditions. $V_T$ is the thermal wind vector for the layer (O—$H_i$), $V_{gh}$ the geostrophic wind at $z = h$ (see section 7.1).

Comparison between the two Richardson numbers (obtained in two independent ways) shows the following:

— Lettau's method (eq. 25) does not work in stable conditions as it gives negative values of $Ri_z$. This can be expected, since in stable conditions convective activity is negligible, so the balance assumed in the derivation of eq. (25) is not valid.

— There is very good agreement between $Ri_z$ and $\overline{Ri}_z$ for unstable conditions in the range 171°—360°.

— The contradiction between $Ri_z$ and $\overline{Ri}_z$ for the group (0°—80°) in unstable conditions is probably connected with the unrealistic values of the drag coefficients and stress (the cross-isobar angle is also too large).

TABLE 7. Various parameters computed for different stratifications. $N$ is the number of profiles included in the mean, $V_s$ (in $m/s$) the surface wind velocity, $G_0$ ($m/s$) the surface geostrophic wind velocity, $\alpha_0$ the cross-isobar angle, $\Delta\alpha_{500}$ the wind veering angle at 500 m, $C_d$ the drag coefficient, $C_g$ the geostrophic drag coefficient, $\tau_0$ (Dynes/cm$^2$) the surface stress, $Ri_s$ the Richardson number defined by equation (25), $\overline{Ri_s}$ the mean surface Richardson number defined by eq. (3) and $H_i$ the upper height of integration (in metres).

| SEA SURFACE | WATER STABLE | | | ICE | | | | | | WATER UNSTABLE | | | | |
|---|---|---|---|---|---|---|---|---|---|---|---|---|---|---|
| DIRECTION GROUPS | 171°—240° | 241°—290° | 291°—360° | 0°—80° | 81°—109° | 110°—170° | 171°—240° | 241°—290° | 291°—360° | 0°—80° | 110°—170° | 171°—240° | 241°—290° | 291°—360° |
| $N$ | 26 | 24 | 15 | 11 | 4 | 6 | 9 | 10 | 16 | 43 | 9 | 11 | 16 | 38 |
| $V_s$ | 7.7 | 6.9 | 7.0 | 7.5 | 6.7 | 8.9 | 7.3 | 7.2 | 7.1 | 7.7 | 9.9 | 7.8 | 7.2 | 8.8 |
| $G_0$ | 9.4 | 11.5 | 9.4 | 8.2 | 10.2 | 13.6 | 10.4 | 9.4 | 10.8 | 12.1 | 12.2 | 9.2 | 9.6 | 10.6 |
| $\alpha_0$ | 27.6° | 37.0° | 17.0° | 16.0° | 21.9° | 15.1° | 18.5° | 30.0° | 22.4° | 33.7° | 19.3° | 12.5° | 14.3° | 2.3° |
| $\Delta\alpha_{500}$ | 33.0° | 40.6° | 17.7° | 12.0° | 27.7° | 18.5° | 17.5° | 30.8° | 9.8° | 4.2° | 6.3° | 17.6° | 11.1° | 7.7° |
| $C_d \times 10^3$ | 0.49 | 1.59 | 0.92 | 0.36 | 1.82 | 1.64 | 0.07 | 0.81 | 3.18 | 10.27 | 4.94 | 0.93 | 3.12 | 1.08 |
| $C_g \times 10^3$ | 0.33 | 0.57 | 0.51 | 0.31 | 0.79 | 0.69 | 0.03 | 0.47 | 1.36 | 4.18 | 3.26 | 0.66 | 1.75 | 0.74 |
| $\tau_0$ | 0.35 | 0.90 | 0.54 | 0.24 | 1.00 | 1.55 | −0.04 | 0.50 | 1.92 | 7.34 | 5.86 | 0.68 | 1.92 | 1.00 |
| $Ri_s$ | −1.65 | −0.12 | 0.02 | 2.08 | 0.01 | −0.26 | 7.50 | −0.37 | 0.15 | 0.04 | −0.03 | −0.48 | −0.20 | −0.39 |
| $\overline{Ri_s}$ | 0.20 | 0.20 | 0.09 | — | — | — | — | — | — | −0.85 | −0.30 | −0.48 | −0.10 | −0.43 |
| $H_i$ | 2 000 | 1 500 | 2 000 | 1 800 | 2 000 | 2 000 | 2 000 | 1 900 | 2 000 | 2 000 | 2 000 | 2 000 | 2 000 | 2 000 |

— In ice situations the mean value of $Ri_s$ for all direction groups indicates an overall stable case. This is in contradiction to the conclusion reached in sections 3 and 4.2. Perhaps a more suitable conclusion as regards the governing stability condition in a sea-ice situation is that it is near-neutral.

One can of course wonder whether the results are sensitive to the choice of $H_i$. This was not the case as long as the upper parts of the profiles were smooth. In a few cases, the two or three upper wind values were deleted, since a decrease in the number of available data led to a marked kink in the mean profile. The resulting value of the upper height of integration is reported in Table 7. As to the very high value of $C_d$ or $\tau_0$ found for the (0°—80°) direction group in unstable conditions, it originates from the computation of the u-profile slope at $z = Z^*$ (cf. eq. 17), which was very small in that case and thus liable to great uncertainty. However, it is also evident from the hodograph that this profile was profoundly disturbed and far from the conventional Ekman spiral. In this connection, one can also notice that the magnitude of deformation of the hodographs from theoretical Ekman spirals is proportional to the strength of the thermal wind and that the axis of deformation corresponds well to the thermal wind direction.

There is another factor affecting the quality of the results, namely, the fact that second-order quantities are not linear with respect to the operation of averaging, i.e.

$$\overline{V}^2 \leq \overline{V^2}$$

Thus the use of average profiles in our computations will lead to smaller values for the drag coefficients.

## 5.3. INTRINSIC EFFECT OF BAROCLINICITY

We shall now try to estimate the effect of baroclinicity alone on the structure of the atmospheric boundary layer. It is well known that the main factor determining the effect of the thermal wind, apart, of course from its magnitude, is its orientation relative to surface isobars or actual wind.

With the assumption of constant geostrophic shear, we obtained, in section 5.1, the components of the thermal wind denoted by $S_u$ and $S_v$, where $S_u$ is the projection of the thermal wind $V_T$ on an x-axis aligned with the surface wind and $S_v$ is its normal component in a direct rotation of the axis. Actually, $S_u$ and $S_v$ should be multiplied by a factor corresponding to the depth of the layer for which $V_T$ is calculated in order to have the real thermal wind. From these data we obtain the modulus $S_0$ of the thermal wind and its direction $\alpha_T$ taken as the direction from which it blows as in normal meteorological practice. We also compute the angle $\beta_s = (\alpha_T - \alpha_s)$ between the surface wind and thermal wind, measured clockwise from the direction of the former to the direction of the latter; the angle $\beta_0$ between the surface geostrophic wind and thermal wind, $\psi = (\alpha_T - \alpha_{500})$, which is the angle measured clockwise from the direction of the wind at $z = 500$ m to the direction of the thermal wind in the lowest 2 km or so. These quantities are represented schematically in Fig. 16.

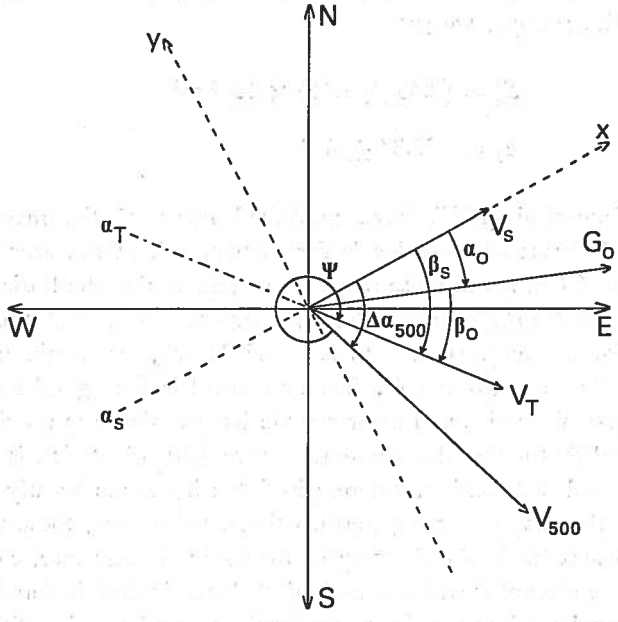


Fig. 16. Schematic representation of the different angle concepts used.

The values for each direction and stability group are given in Table 8. With the axis chosen, a warm advection occurs when the angle $\psi$ is in approximately the range (0°, 180°), with a maximum at $\psi = 90°$, whereas there is a cold advection for values of $\psi$ in the range (180°, 360°), which reaches its maximum when $\psi = 270°$.

TABLE 8. Various baroclinicity parameters as functions of wind direction group and thermal stability. $N$ is the number of runs; $S_u$, $S_v$ and $S_0$ the two components and the modulus of the thermal wind respectively; $\psi = (\alpha_T - \alpha_{500})$; $\beta_s = -\tan^{-1}(S_v/S_u)$; $\alpha_T = (\alpha_s + \beta_s)$; $\beta_0 = (\beta_s - \alpha_0)$.

| SEA SURFACE | WATER STABLE | | | ICE | | | | | | WATER UNSTABLE | | | | |
|---|---|---|---|---|---|---|---|---|---|---|---|---|---|---|
| DIRECTION GROUPS | 171°—240° | 241°—290° | 291°—360° | 0°—80° | 81°—109° | 110°—170° | 171°—240° | 241°—290° | 291°—360° | 0°—80° | 110°—170° | 171°—240° | 241°—290° | 291°—360° |
| $N$ ..... | 26 | 24 | 15 | 11 | 4 | 6 | 9 | 10 | 16 | 43 | 9 | 11 | 16 | 38 |
| $S_u \times 10^3$ | −0.61 | −0.51 | 0.81 | 3.22 | −3.73 | −3.85 | −2.85 | 1.57 | 0.25 | −0.97 | 0.52 | 0.69 | −1.54 | 1.98 |
| $S_v \times 10^3$ | −1.46 | −0.28 | −0.20 | 0.64 | 1.56 | −0.60 | 0.65 | −1.61 | 1.64 | 4.19 | −2.06 | −1.44 | −2.10 | −1.67 |
| $S_0 \times 10^3$ | 1.58 | 0.58 | 0.83 | 3.28 | 4.05 | 3.89 | 2.92 | 2.25 | 1.66 | 4.30 | 2.12 | 1.60 | 2.60 | 2.59 |
| $\alpha_T$ .... | 328° | 60° | 342° | 16° | 292° | 326° | 35° | 308° | 251° | 285° | 207° | 268° | 26° | 18° |
| $\beta_s$ ..... | 113° | 151° | 14° | 349° | 203° | 171° | 193° | 46° | 279° | 257° | 76° | 64° | 126° | 40° |
| $\psi$ ..... | 80° | 110° | 356° | 337° | 175° | 153° | 175° | 15° | 269° | 253° | 69° | 47° | 115° | 32° |
| $\beta_0$ ..... | 85° | 114° | 357° | 333° | 181° | 156° | 175° | 16° | 257° | 223° | 57° | 52° | 112° | 38° |

If we average the values obtained for the intensity and direction of the thermal wind over all the groups, we get:

$$S_0 = (2.45 \pm 1.15) \times 10^{-3}\ \mathrm{s}^{-1}$$

$$\alpha_T = 325.8° \pm 61°$$

Guterman & Hanevskoi (1963) have published maps of the mean temperature distribution at different pressure levels for each month of the year averaged over the period 1950—1956. From these maps we can determine the horizontal temperature gradient over the study area and thus compute the thermal wind. Taking the level 850 mb for the months of February and March, we obtain mean values of $S_0 \approx 1.02 \times 10^{-3}\ s^{-1}$ and $\alpha_T \approx 316°$. The agreement is very good for the direction of the mean thermal wind, but in our sample its magnitude is much greater. This may be explained by the fact that the temperature field orientation is mainly characterized by its zonal distribution, whereas its intensity varies greatly and may have large values in the case of strong perturbations. Of course, these values are also affected by inaccuracies in the drawing of the maps. In any case, this rather good agreement between the observed climatological thermal wind field and the computed mean field of our data gives some support for the general validity of the assumptions used in its computation.

An attempt can now be made to express the results of section 5.2 for the wind stress and drag coefficients as a function of the baroclinicity parameters $S_0$, $\beta_s$, $\beta_0$ or $\psi$.

The dependence on $\psi$ is the easiest to interpret in terms of thermal wind, but as the surface geostrophic wind or even the actual surface wind are more easily available from the usual routine forecasts or observations, the dependence on $\beta_0$ or $\beta_s$ might be more useful. However, the change from one to another does not greatly affect the general aspect of the curves. The cross-isobar angle $\alpha_0$ is shown in Fig. 17a and b as a function of $\psi$ and $\beta_0$, respectively.

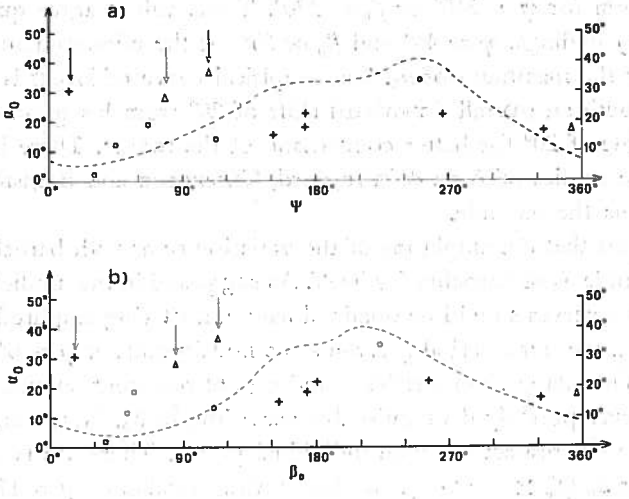


Fig. 17. Variation of the cross-isobar angle with a) the angle between the thermal wind and the wind at 500 m, b) the angle between the thermal wind and the surface geostrophic wind. Triangles are for stable conditions, crosses for ice situations and open circles for unstable conditions. The arrows point the very stable mean runs. The dashed curves represent the corresponding results of Hoxit (1974).

The interpretation of these curves is somewhat difficult since there are only 14 empirical points; moreover the effects of baroclinicity and stability are superimposed on each other, and, in addition, each of them has a different magnitude for each point. However, it is possible to distinguish a sine-like trend with smaller values of $\alpha_0$ for warm air advection cases (i.e. $\psi = (0°, 180°)$) and larger values for cold air advection. Since the points corresponding to a stable state (shown by an arrow in the figures) have very large values, the whole curve $\alpha_0 = F(\psi$ or $\beta_0)$ should then probably be shifted upwards. For cases of parallelism ($\psi \approx 0°$) or antiparallelism ($\psi \approx 180°$) of the actual flow with the thermal wind, the observed points are close to the overall mean value of $\bar{\alpha}_0 = 20.5°$. Thus, in conclusion, the effect of baroclinicity on the cross-isobaric angle appears as a sine-function with an amplitude of approximately

15°. The nodal points are separated by a $\pi$-phase and correspond to the alignment of the thermal wind along or against the actual wind. These results agree with results obtained theoretically by Arya & Wyngaard (1975) with a higher-order closure model (cf. their Fig. 10), by Thompson (1974) with a simple model of the baroclinic well-mixed layer and empirically by Bernstein (1973) and by Hoxit (1974). As mentioned before, the two curves of Fig. 17a and 17b are very similar, they can be superimposed before, the two curves of Fig. 17a and 17b are very similar, they can be superimposed through a translation of magnitude $\alpha_0$ for the warm air advection range and of magnitude $-\alpha_0$ for the cold air advection range. If a sine-function is fitted roughly by eye to our observation points, $\alpha_0$ reaches a minimum for $\psi \approx 50°$ or $\beta_0 \approx 60°$ and a maximum for $\psi \approx 240°$ or $\beta_0 \approx 220°$. These values agree quite closely with Hoxit's (1974) findings: $\psi \approx 45°$ and $\beta_0 \approx 65°$ for the minimum and $\psi \approx 245°$ and $\beta_0 \approx 210°$ for the maximum of $\alpha_0$. The empirical curve of Hoxit is also plotted in Fig. 17, but with an overall downward shift of 20° from his mean value of 40° to our mean value of 20° for better comparison of the results. There is similar agreement with the studies of Arya & Wyngaard, Thompson and Bernstein, where $\beta_s$ is used instead as the variable.

It is obvious that the amplitude of the variation of $\alpha_0$ with baroclinicity depends on the magnitude $S_0$ of baroclinicity itself. As suggested in the studies quoted above, a family of sine curves should be obtained having a varying amplitude (proportional to $S_0$) but with the same period (i.e. the same nodal points at $\psi \approx 0°$ and 180°). Unfortunately, our data are too restricted and do not represent enough values of $S_0$ to reveal the curves possibly distinguishable according to $S_0$. However, some remarks can be made with respect to some individual points. There are two points with a large value of $S_0$ ($S_0 \times 10^3 > 4$): the one having a value of $\psi = 175°$ (i.e. close to the nodal point) does not show any great departure from the mean value, whereas the other has $\psi = 253°$ (i.e. close to the maximum due to cold air advection) and is clearly larger than all the other observation points, although it corresponds to an unstable situation, which should make it small. Most of the other points are around $2 \times 10^{-3}$, which may explain the reduced scatter. On the other hand, it is impossible to compare our values of $S_0$ with the corresponding parameter of the earlier studies, since they use either the height of the well-mixed convective boundary layer (Arya & Wyngaard) or the Väisälä frequency characteristic of the stable capping layer (Thompson). However, reference to the previous empirical studies shows that the 12Z curve of Hoxit, which corresponds best to our set of data, has an amplitude of 17.5°, and that Bernstein obtains a value close to 15°, which is in good agreement with our value.

One last remark can be made concerning the cross-isobar angle of the surface wind: our data seem to suggest that stability can affect the curve $\alpha_0 = F(\beta_0 \text{ or } \psi)$ by shifting the mean barotropic value around which baroclinicity makes $\alpha_0$ oscillate. This interesting point is difficult to verify, since previous studies do not consider the effect of thermal stability separately but, instead, average over all the data avail-

able, regardless of thermal stability and also of surface roughness. According to the data used, the situations dealt with earlier are probably all near-neutral or unstable. Then our large values of $\alpha_0$ in stable conditions may be explained by the fact that stable stratification, by providing strong resistance to the baroclinic effect, imposes its large value of $\alpha_0$. For instance, stable stratification can be imagined to present an effective barrier to the expected downward transport of additional momentum originating from geostrophic shear (Hoxit 1974), which would normally oppose the flow toward lower pressure, i.e. reduce the cross-isobar angle of the surface wind. Similarly, convective activity produces zero-wind shear profiles in the well-mixed boundary layer, although baroclinicity is present with strong geostrophic shear as was shown by Arya & Wyngaard (1975). This is only a hypothesis, and it should be verified theoretically and especially empirically with a larger amount of data, in which thermal stability conditions are distinguished from baroclinicity conditions.

Next, we shall have a look at the behaviour of wind veering in the lowest half kilometre under baroclinic conditions. The variation of $\Delta\alpha$ (500) as a function of $\psi$ is plotted in Fig. 18. The striking feature is that the veering angle behaves in the opposite way to the cross-isobar angle, having its maximum during warm air advection and its minimum in cold advection. This result is in accordance with those of Hoxit (1974), obtained by processing nearly 23 000 radiosoundings.

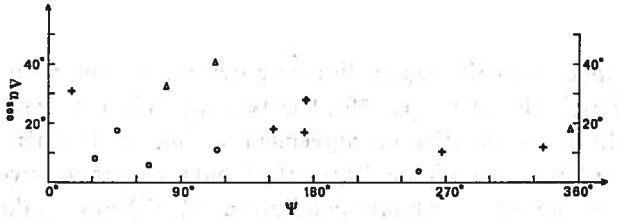


Fig. 18. Dependence of wind veering in the lowest 500 m on the angle between the wind at 500 m and the thermal wind. Triangles are for stable cases, crosses for ice situations and open circles for unstable conditions.

As has been demonstrated by Sheppard et al. (1952), the effect of baroclinicity is not limited to its action on wind veering but it also changes the vertical shear of the horizontal wind in the boundary layer, which in turn modify the turbulent transport of momentum and the stress profiles. This is illustrated in Fig. 19, which shows the effect of baroclinicity on the surface stress normalized by the average surface geostrophic wind of each group. The scatter of the data is greater than for the previous curves, which makes it hazardous to draw any line fitting these points. However, the ratio $\tau_0/G_0$ seems to have a maximum in the range from $\beta_0 \approx 120°$ to $\beta_0 \approx 300°$ (this last value could as well be 270° or 320°, as we lack data in the range (260°, 330°)); the ratio has a decreasing trend from this undefined last value of $\beta_0$ to

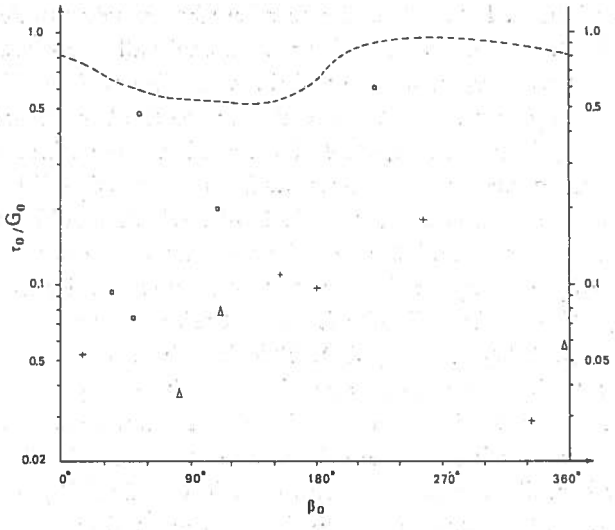


Fig. 19. Dependence of the surface stress normalized by the geostrophic wind on the angle between the surface isobar and the thermal wind in the lowest 2 km. Units are (dynes cm$^{-2}$)/(m sec$^{-1}$). The dashed curve represents the corresponding results of Hoxit (1974).

90°, and then appears to rise again. For comparison, a similar curve obtained by Hoxit (1974) is reproduced in Fig. 19. The two dependences have some common features, but show no quantitative agreement at all, as Hoxit's values for the ratio are one order of magnitude larger than ours, except for two of our points corresponding to unstable stability conditions. Hoxit'stress values are in fact rather high; they vary from 5.6 to 10.5 dynes cm$^{-2}$, whereas Johnson (1962), who also used the geostrophic departure method for stations located in the same study area as Hoxit's, obtained surface stress values in the range 0.64 to 3.44 dynes cm$^{-2}$, i.e. values comparable to the present ones obtained over an island-studded sea. Anyway, both the present results and those of Hoxit show that the stress is strongly dependent on the direction of the thermal wind, with larger values in cold air advection situations.

Another measure of drag is the ratio $V_s/G_0$, which is shown in Fig. 20. The scatter of the observation points is remarkably small and there is no distinct differentiation due to thermal stability. The corresponding curve of Hoxit has also been plotted in the figure for comparison. Hoxit's curve has been representated with an overall upward shift of 0.23 from his mean value of 0.51 to our mean value 0.74. These two curves are rather similar to Hoxit's curve for the normalized downwind surface stress shown in Fig. 19. The maximum now occurs in the region close to $\beta_0 = 0°$. In other words, the additional downward momentum transfer induced by

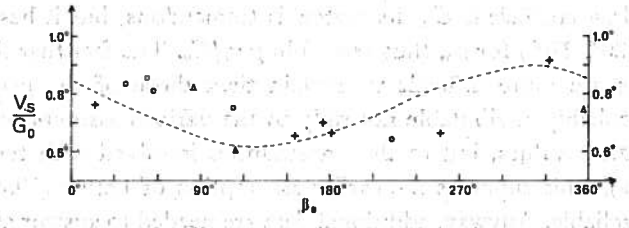


Fig. 20. Dependence of the ratio $V_s/G_0$ on the thermal wind direction with respect to surface isobars. Triangles are for stable cases, crosses for ice situations and open circles for unstable cases. The dashed curve represents Hoxit's (1974) results.

the geostrophic shear results, for a given geostrophic wind, in an increase of the surface wind speed and a slight decrease of the cross-isobar angle (cf. Fig. 17). This shows that barotropic conditions do not correspond to a baroclinic case with a zero $\beta_0$ angle.

Since the geostrophic drag coefficient $C_g$ is a factor commonly used in boundary layer parameterization, it is also interesting to observe its behaviour as a function of the thermal wind direction. This is shown in Fig. 21, where 3 very high values of $C_g$ for unstable conditions fall outside the order of magnitude of the majority of the other values. This figure shows a clear variation of $C_g$ with $\beta_0$, with a maximum at $\beta_0 \approx 270°$ (cold air advection) and a minimum at $\beta_0 \approx 90°$.

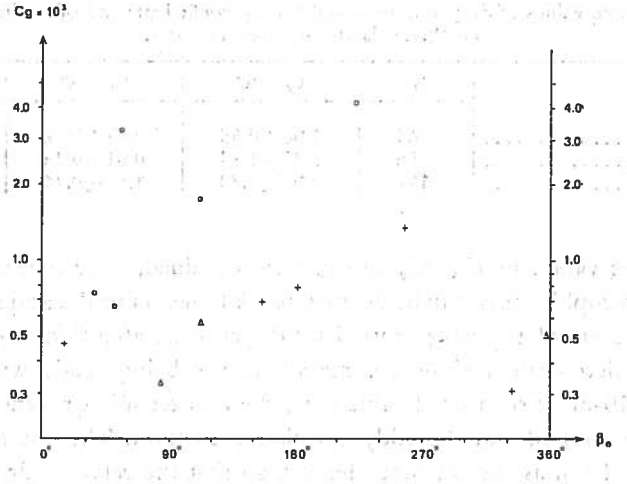


Fig. 21. Dependence of the geostrophic drag coefficient on the angle between the thermal wind and the surface isobars. Triangles are for stable cases, crosses for ice situations and open circles for unstable cases.

As to the drag coefficient $C_d$, its scatter is tremendous, but it has higher values in the range (120°, 270°) for $\beta_0$, thus resembling $\tau_0/G_0$. The fact that the drag coefficient variations are more difficult to explain than those of the geostrophic drag coefficient is probably attributable not only to the various assumptions made in the derivation of these values, but to the uncertainties involved with the surface wind (all local effects). This supports the earlier assumption of Lettau (1959) that the use of $C_g$ is more reliable. Anyway, additional data are needed to answer all the unsolved questions.

## 6. DRAG COEFFICIENTS AND SURFACE STRESS

Since this study was prompted by the need to parameterize surface stress for its inclusion in the ice-drift model, this section will be devoted to some aspects of this problem.

The scatter of the values of $C_d$, $C_g$ and $\tau_0$ presented in Table 7 may be reduced by averaging them over all the direction groups, so that mean values are obtained for the three stratification groups, stable, unstable and ice (see Table 9). The values obtained fall in the expected range of magnitude. An extensive literature exists on the value of the drag coefficient (generally at reference height 10 m) over open water. Measurements on ice floes were initiated a few years ago, mainly at the instigation of the Arctic Ice Dynamics Joint Experiment (AIDJEX).

TABLE 9. Average values of drag and geostrophic drag coefficients and of surface stress (in dynes $cm^{-2}$). $N$ is the number of cases.

| | N | $C_d \times 10^3$ | $C_g \times 10^3$ | $\tau_0$ |
|---|---|---|---|---|
| Stable | 65 | $1.00 \pm 0.55$ | $0.47 \pm 0.12$ | $0.60 \pm 0.28$ |
| Ice | 56 | $1.31 \pm 1.14$ | $0.61 \pm 0.46$ | $0.86 \pm 0.77$ |
| Unstable | 117 | $4.07 \pm 3.80$ | $1.56 \pm 0.74$ | $3.36 \pm 3.04$ |

The present values of $C_d$, $C_g$ and $\tau_0$ were obtained, after several assumptions, from the ageostrophic mass flux in the lowest 2 kilometers of the atmosphere. However, in assessments of the drag exerted by the surface, attention is often restricted to small or micro-scale turbulence, measurements being made with instruments attached to a 10-m or so mast. In this case, the two techniques generally employed are the profile method and the eddy correlation method. The common practice is to choose $z = 10$ m as the reference height, so that the relevant drag coefficient is defined by the relation.

$$C_{10} = (u_*/V_{10})^2 \tag{26}$$

As the neutral wind profile is logarithmic close to the surface, a large amount of data exists for neutral or nearly neutral stability conditions, especially for the profile method.

Thermal stability may be taken into account by adding a function $\Phi$ of stability to the neutral logarithmic law, so that

$$u(z) = (u_*/\kappa)\left[\ln(z/z_0) + \Phi(z/L_*)\right] \tag{27}$$

where $u_*$ is the friction velocity and $L_*$ the so-called Monin-Obukhov stability length. The strong dependence of this function $\Phi$ on the degree of stability (Businger et al. 1971) and the fact that there is still some disagreement about its analytical expression (Yaglom 1977) explain why neutral conditions have been favoured so far.

## 6.1. DRAG COEFFICIENTS OVER WATER

Some of the principal results for the determination of $C_{10}$ over the sea as a function of $V_{10}$ are shown in Fig. 22 from Smith & Banke (1975).

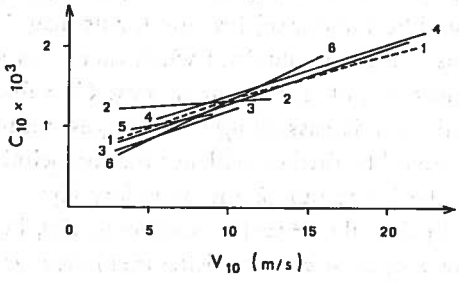


Fig. 22. Drag coefficient and wind speed: (1) solid, Smith & Banke (1975); (1) dashed, with Charnock's (1955) formula; (2) Brocks & Krügermeyer (1970); (3) Hasse (1968); (4) Miller (1964); (5) Miyake et al. (1972); (6) Sheppard et al. (1972). After Smith & Banke (1975).

Although the dispersion of the individual measurements is great, the mean drag coefficient values fall mainly between $10^{-3}$ and $2 \times 10^{-3}$.

As to the dependence on thermal stability, it has been shown that the drag coefficient increases with the degree of instability.

Confirmation of the importance of the stability effect can be found in studies of the state of the sea in relation to wind speed and the air-sea temperature difference. For instance, Roll (1952) found that, for a given wind speed, the mean wave height when $(T_a - T_w) = -6.7°C$ is 22% greater than when $(T_a - T_w) = 0$. Brown (1953) and Fleagle (1956) have reported effects of similar magnitude.

On the basis of recently published results, Hsu (1974) proposed the following empirical relation:

$$\kappa/(C_{10})^{\frac{1}{2}} = 11.5 + 4.36\ (z/L_*) \tag{28}$$

where $\kappa$ is the Von Karman constant and $z/L_*$ the stability parameter. In order to compare the results shown in Table 9 with those predicted by formula (28), we must relate our stability coefficient $Ri_*$ to the parameter $z/L_*$. For this we must use the results obtained for the assessment of the flux-profile relationships (e.g. Pruitt et al. 1973). The values for $z/L_*$ corresponding to our overall $Ri_*$ values of 0.162 (stable) and —0.432 (unstable) are 0.203 and —0.315 respectively. According to Hsu's regression formula, these values give $1.04 \times 10^{-3}$ and $1.55 \times 10^{-3}$ for $C_d$ in the stable and unstable cases, respectively, i.e. an increase of 50%. The stable value of $C_d$ is close to ours but the unstable one is much lower than ours. From water tilt observations, Darbyshire & Darbyshire (1955) obtained a value of $C_d$ ($z = 12$ m) as high as $3.2 \times 10^{-3}$ in certain unstable cases, but unfortunately their paper does not provide precise information on a stability parameter. So, our value of $C_d$ for unstable conditions seems to be too high as compared with the results of other studies, but one must not forget the assumptions made to obtain these values and the uncertainty regarding the quality of the surface wind data. Mention may be made, however, of a value for $C_d$ as high as $12 \times 10^{-3}$ obtained by Holopainen (1961) from aerological observations over Jackson (Alab.). Although this value was obtained over land, it is much greater than might be expected, so there should be some special reason for its magnitude. This may possibly be the fact that this value was obtained when there was a strong horizontal temperature gradient. It may be noted that our highest $C_d$ value ($= 10.27 \times 10^{-3}$) occurs for the case where the winds pass along the strongest mean temperature gradient (northeasterlies). This would be further evidence that baroclinicity is one of the major factors influencing the behaviour of the boundary layer.

The drag coefficients $C_d$ or $C_{10}$ depend primarily on surface characteristics, i.e. are local parameters, but, like the state of the sea, these characteristics themselves are non-local phenomena. This contradiction is probably one of the main reasons for the great variation of $C_{10}$. This makes it seem natural to introduce a geostrophic drag coefficient as defined in eq. (24), thus relating surface drag to the large-scale forcing velocity, i.e. the geostrophic wind.

Our values of $C_g$ agree well with Deacon's (1973) finding of $0.73 \times 10^{-3}$ at sea, and Brocks & Krügermeyer's (1972) observed value of $0.6 \times 10^{-3}$, whereas a smaller value, $0.48 \times 10^{-3}$, was obtained for the Scilly and Helgoland pibal profiles (Lettau, 1957; Lettau & Hoeber, 1964), using the ageostrophic method for a near-neutral situation. Hasse & Dunckel (1974) also found a slight increasing trend for $C_g$ with increasing instability. Wippermann (1972b) predicted values of $C_g$ using a barotropic model based on the resistance laws for the planetary boundary layer; the values in

stability conditions corresponding to the present ones varied from $0.3 \times 10^{-3}$ in the stable case to $2.3 \times 10^{-3}$ in unstable conditions, so there is qualitative agreement with our results. Our values of $C_g$ show an increasing trend with increasing surface geostrophic wind velocity $G_0$, but the correlation coefficient of the regression is only 0.57.

It is interesting to note that the standard deviation for $C_g$ is less than for $C_d$, although the geostrophic drag coefficient does not depend only on surface characteristics like $C_d$, but also on those of the whole boundary layer, e.g. stability, baroclinicity, unsteadiness. Therefore, it seems more reliable to use a geostrophic drag coefficient for the parameterization of the surface stress, especially as the geostrophic wind required for the ice-drift model may be obtained directly from a weather forecasting model.

## 6.2 DRAG DETERMINATIONS OVER SEA ICE

The number of available wind stress measurements made over sea ice is rather limited. The first article on the subject was published as late as 1965. A survey of the first results obtained is given by Joffre (1975) and the most recent measurements are reviewed by Banke et al. (1976). All these results are difficult to compare, since they were obtained on different floes with different topographical characteristics. Sea ice always presents irregularities owing to the pressure forces which drive the ice-floes against, over and under each other. These »larger-scale» features of sea ice may be taken into account in the assessment of the wind drag through the introduction of a form drag concept, which is added to the habitual surface drag (Arya 1975b; Banke & Smith 1973).

The surface drag, which depends on the small-scale morphology of the ice, is subject to frequent change. The surface features may be modified by new snowfalls, the formation of snow drifts and sastrugi (sharp, irregular ridges formed on a snow surface by wind erosion and deposition) under wind action, rain during a warm period, which leads to firnification of the snow cover, and the metamorphosis of the snow cover by absorption of solar radiation. Thus, the aerodynamic small-scale roughness parameters are sensitive functions of all these changes. However, although the values reported for $C_{10}$ do vary widely, they fall in the same range as those for open-sea situations, i.e. between $10^{-3}$ and $2 \times 10^{-3}$. The stability effect has also been observed, with higher values for unstable cases ($C_{10} = 3.7 \times 10^{-3}$ reported by Smith et al. 1970) and smaller values in stable situations ($C_{10} = 0.5 \times 10^{-3}$ Banke et al. 1976). A sample of neutral-stability drag coefficients is shown in Table 10.

TABLE 10. Ice surface parameters for neutral stability (from Banke et al. 1976).

| Location | Year | $C_{10} \times 10^3$ | $\zeta$ (cm) |
|---|---|---|---|
| Gulf of St. Laurence | 1970 | 1.42 | — |
| Beaufort Sea | 1971 | 1.68 | 5.6 |
| | 1971 | 1.51 | 5.5 |
| Arctic Ocean | 1972 | 1.82 | 9.8 |
| | 1972 | 1.56 | 6.3 |
| Robeson Channel | 1972 | 2.08 | 13.2 |
| | 1974 | 1.65 | 6.5 |
| Beaufort Sea | 1975 | 1.38 | 4.6 |
| flat | 1975 | 1.57 | 7.0 |
| hummocked | 1975 | 1.62 | 9.7 |

A useful parameter has been introduced in these studies: a so-called surface elevation parameter $\zeta$, which is obtained by integrating a power spectrum of surface elevation

$$\zeta^2 = \int_{k_0}^{\infty} \varphi_s(k)\, dk$$

where $\varphi_s(k)$ is a wave number spectrum of surface elevation, $k$ the downwind radian wave number and $k_0$ a cut-off wave number. The spectrum of surface elevation is obtained from upwind profiling. Taking the surface elevation $\zeta$ as a descriptive parameter, Banke et al. (1976) show the dependence of $C_{10}$ on $\zeta$ and fit the points with a regression line. This regression explains the dependence of the drag on the surface elevation parameter rather well, but it is likely that other parameters, such as spacing or steepness of the roughness elements, can be just as important in determining the drag coefficient.

## 7. PRESENTATION OF THE UTÖ DATA IN THE FRAMEWORK OF THE SIMILARITY THEORIES

### 7.1 THE VELOCITY-DEFECT LAWS

In the previous sections we have seen that the behaviour of the wind profile in the atmospheric boundary layer is very variable and depends on many factors. The estimation of the relative importance of each of these factors and of their quantitative effect on the vertical structure of the wind seems therefore a hopeless task. Recently, however, considerable advances have been made in the understanding and detailing of the planetary boundary layer structure, through the use of so-called similarity theories, from which the resistance laws are derived (e.g. Kazanski & Monin, 1960; Csanady, 1967; Blackadar & Tennekes, 1968; Gill, 1968; Clarke, 1970, and Yordanov & Wippermann, 1972).

By choosing the relevant parameters acting on the structure of the planetary boundary layer, it is possible to form relationships between dimensionless combinations of these parameters giving the vertical structure of wind, temperature and moisture distribution in the boundary layer. The relevant internal parameters playing a role in the behaviour of the planetary boundary layer are listed below (for a review see Kitaigorodskii & Joffre, 1976):

$$z, u_*, Q_0, g\beta, f, h, z_0 \tag{29}$$

where h is the actual height of the boundary layer and $Q_0$ is the surface kinematic heat flux ($= \overline{w'\theta'}_0$); the other parameters having the same meaning as in the previous sections. Baroclinic effects can also be included, but at the cost of taking two additional parameters, $S_u = \partial U_g/\partial z$ and $S_v = \partial V_g/\partial z$ (cf. Yordanov & Wippermann, 1972; Wippermann, 1972a; Clarke & Hess, 1974).

According to Buckingham's $\pi$-theorem, it is possible to form six independent dimensionless parameters on which the dependent variables describing the planetary boundary layer (e.g.: $u$, $v$, $\Theta$, $q$, $K_m$, $\tau$, ...) depend:

$$\begin{aligned} &z/h,\ h/z_0,\ \zeta_h = h/L_*,\ \mu_h = hf/u_* \\ &S_x = S_u(h/u_*),\ S_y = S_v(h/u_*) \end{aligned} \tag{30}$$

The use of the actual height h of the boundary layer as a scaling height has been suggested by the results of numerical simulation of the planetary boundary layer by Deardorff (1970 a, b; 1972a), since this height (or the height $z_i$ of the base of the inversion capping the convective boundary layer) appears to scale properly, in contrast to the height $\Lambda = Ku_*/f$ proposed in earlier studies. But, since $\Lambda$ is of the same order of magnitude as h and scales the neutral planetary boundary layer well, it should also be included and, instead of the often used dimensionless parameter $\mu_0 = \Lambda/L_*$, we use the ratio of these two scaling heights, i.e. $hf/u_*$, as suggested by Arya & Wyngaard (1975). An additional advantage of this parameter is that it does not present singularities with respect to latitude.

As we are interested in the velocity defect between geostrophic and actual wind and wish to eliminate baroclinic effect at the first stage, for the sake of simplicity, we can write:

$$\frac{U_{gh} - u(z)}{u_*} = \Psi_u(z/h,\ h/z_0,\ \zeta_h,\ \mu_h) \tag{31a}$$

$$\frac{V_{gh} - v(z)}{u_*} = \Psi_v(z/h,\ h/z_0,\ \zeta_h,\ \mu_h) \tag{31b}$$

where $\Psi_u$ and $\Psi_v$ are unknown dimensionless functions to be determined. We recall

that we are dealing with a coordinate system whose x-axis is aligned along the surface wind. By considering the asymptotic behaviour of these functions, we can eliminate some of the arguments. If we take the case of a well-developed boundary layer, where $h/z_0 \gg 1$, the dependence on this parameter is smoothed out, and the functions $\Psi_u$ and $\Psi_v$ in eqs. (31) depend on three parameters only.

The only unknown is now the height h of the boundary layer. Different methods may be adopted for assessing h, the simplest being to assume h constant and fixed at a certain height, as was done by Zilitinkevich & Chalikov (1968), with h = 1000 m, or in sections 4.2 and 4.3 of this study with h = 500 m. However, the height h is not a stationary quantity; it has a diurnal cycle (e.g. Clarke et al., 1971) and stability-dependent behaviour (Zilitinkevich, 1972).

In the unstable cases, the height h of the boundary layer can be determined fairly easily from the vertical profile of the virtual potential temperature, which shows a fairly homogeneous distribution within the well-mixed convective layer and is topped by an inversion. The base of this inversion corresponds to the height of the boundary layer (Deardorff, 1972a; Wyngaard et al., 1974; Melgarejo & Deardorff, 1974) but at this level geostrophic equilibrium is not reached, adjustment occurring only above the inversion. Another clue to the height of the unstable boundary layer is provided by the shape of the wind profile, which generally undergoes a sudden change at the level of the inversion (Arya & Wyngaard, 1975). Since no temperature profile is available in this case, these various clues will be used for the determination of h in unstable conditions.

In the stable cases, h can be taken as either the height of the maximum of $u(z)$ (Melgarejo & Deardorff, 1974; Clarke 1970) or the height of the minimum of $u(z)$ (Businger & Arya, 1974). The former is, however, only about half of the latter and, since there is still a considerable amount of lateral stress and velocity defect remaining at this level, it has been claimed that it should not be considered the top of the boundary layer (Businger & Arya, 1974). With our knowledge of the computed geostrophic wind profile, our data support this affirmation.

The height h of the boundary layer was determined according to these considerations for the 14 average profiles selected in section 5.2. The geostrophic wind components $U_{gh}$ and $V_{gh}$ at this height were determined from the knowledge of the geostrophic shear presented in Table 8, and the vector $V_{gh}$ is shown in the hodographs of Fig. 15.

Figs. 23 and 24 show the non-dimensional profiles for the two components $(U_{gh}-u)/u_*$ and $(V_{gh}-v)/u_*$, respectively, distinguishing the three stability (stable, ice and unstable) and the directional groups. Comparison of the stable and the unstable profiles shows, as expected, that the overshooting in the longitudinal velocity-defect profiles is stronger and occurs at lower levels for the stable than for the unstable cases, and that the lateral velocity-defect profiles show greater variability in stable than in unstable conditions. The values of h, $\overline{Ri}$, (proportional to $h/L_*$), $hf/u_*$ and the number $N$ of averaged profiles are presented in Table 11.

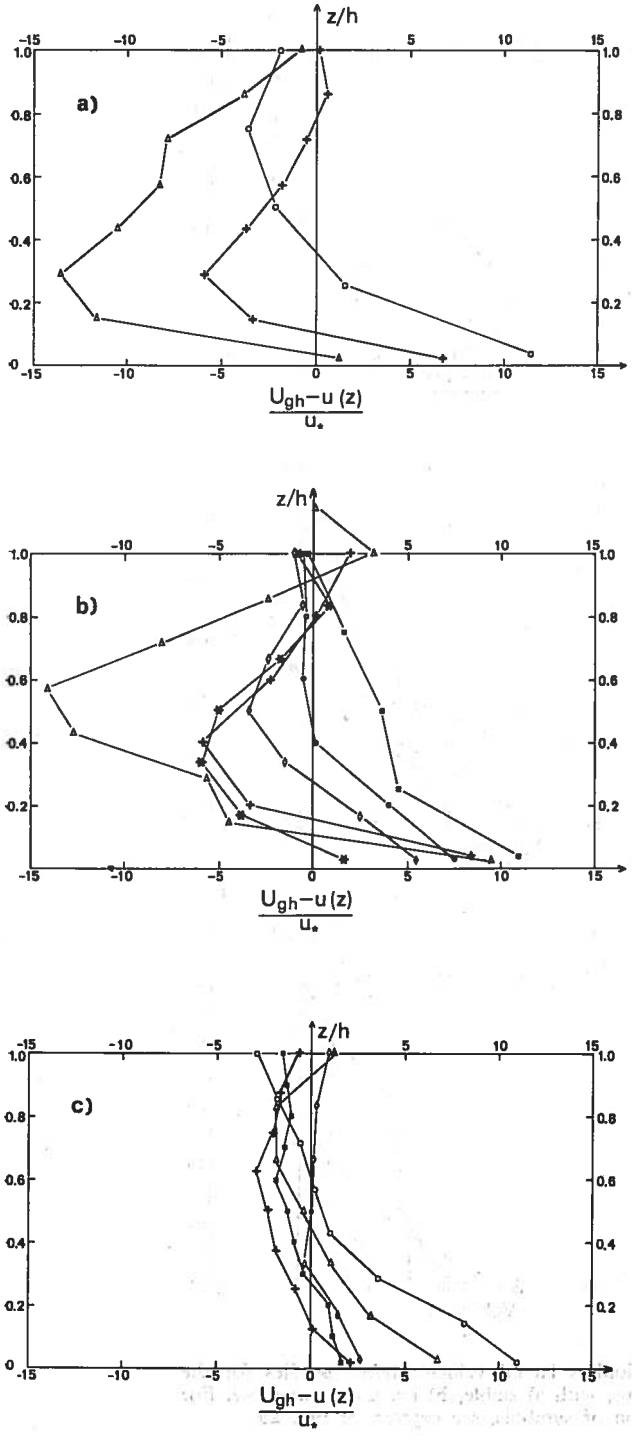


Fig. 23. Dimensionless longitudinal velocity-defect profiles for the 14 selected groups, with a) stable, b) ice and c) unstable. Full squares (■): group 0°—80°; Asterisks (*): group 81°—109°; Diamonds (◇): group 110°—170°; Triangles (△): group 171°—240°; Crosses (+): group 241°—290°; Open circles (○): group 291°—360°.

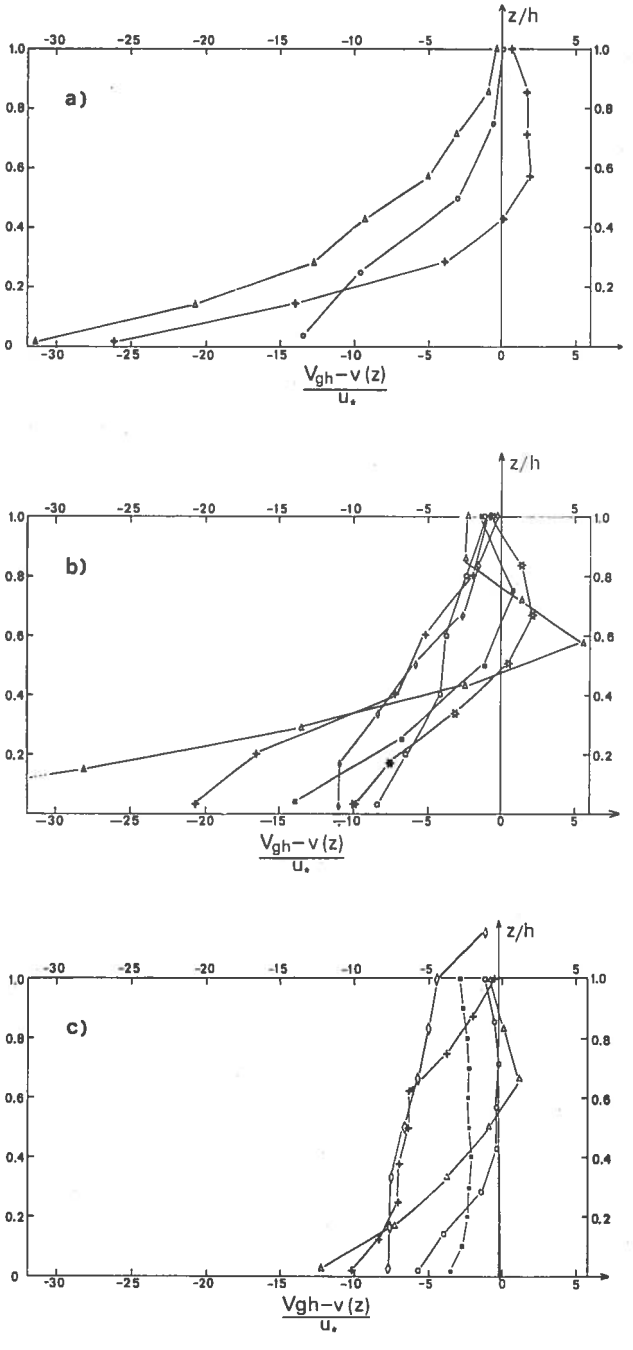


Fig. 24. Dimensionless lateral velocity-defect profiles for the 14 selected groups, with a) stable, b) ice and c) unstable. For explanation of symbols, see caption of Fig. 23.

TABLE 11. Values of the boundary layer height h, the stability parameter $\overline{Ri}_*$ and the similarity parameter $hf/u_*$ for the selected mean profiles.

| Groups | | N | h | $\overline{Ri}_*$ | $hf/u_*$ |
|---|---|---|---|---|---|
| stable ..... | 171°—240° | 26 | 700 | 0.20 | 0.52 |
| | 241°—290° | 24 | 700 | 0.20 | 0.32 |
| | 291°—360° | 15 | 400 | 0.09 | 0.24 |
| ice ..... | 0°—80° | 11 | 400 | — | 0.35 |
| | 81°—109° | 4 | 600 | — | 0.26 |
| | 110°—170° | 6 | 600 | — | 0.21 |
| | 171°—240° | 9 | 700 | — | 1.45 |
| | 241°—290° | 10 | 500 | — | 0.25 |
| | 291°—360° | 16 | 500 | — | 0.16 |
| unstable ..... | 0°—80° | 43 | 1 000 | —0.85 | 0.16 |
| | 110°—170° | 7 | 600 | —0.30 | 0.11 |
| | 171°—240° | 11 | 600 | —0.48 | 0.32 |
| | 241°—290° | 16 | 800 | —0.10 | 0.25 |
| | 291°—360° | 38 | 700 | —0.43 | 0.30 |

When the influence of the magnitude of the stability parameter is considered, it is seen that the shape of the less stable of the stable profiles (group 291—360) tends toward the shape of the unstable profiles. Alhough $Ri_*$ is not available for the ice profiles, some conclusions about the stability conditions can be drawn from the aspect of the profiles; the groups (171°—240°) and (241°—290°) show stable characteristics and the groups (291°—360°), (0°—80°) and (110°—170°) show unstable characteristics. This is what is expected if the dependence shown in Fig. 5 is assumed to apply in ice conditions as well. The group (81°—109°) is somewhere between the two stability classes.

The effect of the second similarity parameter $hf/u_*$ is more difficult to discern since its values range within a limited domain. So far, with our data, a possible influence has been evident only in connection with the lateral velocity-defect profiles. It seems that the vertical gradient of the lateral velocity defect (i.e. the opposite of the lateral stress) increases with increasing value of $hf/u_*$, which is in agreement with the modelling results of Sundararajan (1975) and with a simple consideration of the equations of the conservation of momentum in their stationary and dimensionless form:

$$\frac{fh}{u_*}\left(\frac{v-V_g}{u_*}\right)=\frac{\partial(\tau_{xz}/u_*^2)}{\partial(z/h)} \tag{32}$$

$$\frac{fh}{u_*}\left(\frac{u-U_g}{u_*}\right)=-\frac{\partial(\tau_{yz}/u_*^2)}{\partial(z/h)} \tag{33}$$

which, after integration from the surface to the height h and assuming that the stress vanishes at $z = h$, yield:

$$\int_0^1 \frac{(v-V_g)}{u_*} d(z/h) = \frac{u_*}{fh} \tag{34}$$

$$\int_0^1 \frac{(U_g-u)}{u_*} d(z/h) = 0 \tag{35}$$

where the opposite of the dynamical similarity parameter $\mu_h$ appears in the right-hand side of the first equation.

On the whole, however, when presented in this way, the profiles are easier to classify into the various groups than were the traditional vertical profiles $u(z)$ and $v(z)$.

On the other hand, internal quantities like $u_*$ and $L_*$ are generally unknowns to be determined from the data rather than input parameters. Therefore, it would seem more realistic to develop a similarity theory making use of currently available external parameters. The relevant external parameters are the same as those listed in (29), apart the substitution of $Q_0$ by the temperature difference $\Delta\Theta = \Theta(h) - \Theta(z_0)$ across the boundary layer and of the friction velocity $u_*$ by the wind velocity $V_h$ taken at $z = h$. Forming again dimensionless parameters on which all the dependent variables should depend, one gets:

$$z/h\,,\ h/z_0\,,\ S = g\beta \frac{\Delta\Theta}{f V_h}\,,\ \tilde{h} = hf/V_h \tag{36}$$

The fourth dimensionless parameter is commonly taken as the surface Rossby number $Ro = G_0/(fz_0)$ instead of $\tilde{h}$. But $z_0$ is generally unknown at sea, since it varies with the boundary layer characteristics themselves, and to obtain a parameter equivalent to the one derived with internal parameters, we choose $\tilde{h} = fh/V_h$. Unfortunately, as the quantity $\Delta\Theta$ was not available from our data, it was rather difficult to describe the large scatter of the dimensionless velocity-defect laws

$$D_u(\tilde{h}) = \frac{u(h)-u(z)}{V_h}\ ;\ D_v(\tilde{h}) = \frac{v(h)-v(z)}{V_h} \tag{37}$$

as a function of the only parameter $\tilde{h}$, with $h$ and $z = z_*$ fixed in order to relate $D_u$ and $D_v$ to the explicit quantities $R$ and $\Delta\alpha$ defined in (4) and (5). A theoretical expression based on simple considerations was also derived for $D_u(\tilde{h})$ and $D_v(\tilde{h})$ giving the proper trend of the observation points, but still more complete data are necessary in order to develop appropriate nomograms.

## 7.2 THE RESISTANCE LAWS

The velocity-defect laws in eqs. (31) are supposed to describe the wind structure in the so-called outer layer or spiral layer. Close to the surface, there exists a surface or inner layer where the only relevant parameters are surface characteristics. It is obvious that the profiles in the two layers must match together in some transition layer, since no discontinuity should appear. The mathematical operation of matching the profiles leads to the so-called resistance laws, which give the drag coefficients and the cross-isobar angle as functions of observable parameters. In the barotropic case these resistance laws can be written:

$$\frac{U_{gh}}{u_*} = \frac{1}{\kappa}\left[\ln(h/z_0) - A_h(\zeta_h, \mu_h)\right] \tag{38a}$$

$$\frac{V_{gh}}{u_*} = -\frac{1}{\kappa} B_h(\zeta_h, \mu_h)\ \text{sign}(f) \tag{38b}$$

where $A_h$ and $B_h$ are two dimensionless universal functions of the parameters $\zeta_h = h/L_*$ and $\mu_h = hf/u_*$. Owing to the obvious advantage of having such universal predicting laws, a large amount of the recent (last 10 years) literature on boundary layer meteorology has been devoted to the assessment of these universal functions from empirical data. The results have shown a large scatter but have yielded some insight into the dependence of $A_h$ and $B_h$ on stability (Arya 1975a; Zilitinkevich 1975; Melgarejo & Deardorff 1974).

The determination of $A_h$ and $B_h$ is straightforward from eqs. (38) if we know the roughness length $z_0$. Since no surface layer measurements are available for the site at Utö during the study period, indirect methods must be used. Charnock (1955) has proposed a formula connecting $z_0$ with friction velocity $u_*$ on the basis of dimensional analysis:

$$z_0 = c\frac{u_*^2}{g} \tag{39}$$

where $g$ is the acceleration due to gravity and $c$ a constant to be fitted from observations. Kitaigorodskii (1969) has listed the values of $c$ obtained by different authors, and it seems that $c = 0.035$ fits the data best. Our results for the functions $A_h$ and $B_h$ are shown in Table 12.

The dependence of the functions $A_h$ and $B_h$ on the second dimensionless parameter $\mu_h$ does not emerge from this small amount of data since its range of variation is very small for these 8 cases; moreover, according to Arya & Wyngaard (1975), only $B_h$ is sensitive to $\mu_h$.

TABLE 12. Values of the barotropic similarity functions $A_h$ and $B_h$.

| Groups | | N | $\zeta_h$ | $A_h$ | $B_h$ |
|---|---|---|---|---|---|
| stable ..... | 171°—240° | 26 | 30.9 | —2.73 | 12.58 |
| | 241°—290° | 24 | 31.3 | 2.00 | 10.47 |
| | 291°—360° | 15 | 7.3 | —2.88 | 5.38 |
| unstable ..... | 0°—80° | 43 | —91.6 | 8.39 | 1.29 |
| | 110°—170° | 7 | —24.5 | 5.96 | 3.03 |
| | 171°—240° | 11 | —35.2 | —0.93 | 4.81 |
| | 241°—290° | 16 | —13.6 | 6.16 | 4.02 |
| | 291°—360° | 38 | —38.0 | —1.94 | 2.23 |

The ice situation data have been omitted here, since Charnock's equation (39) for the roughness length is valid only for open-sea situations, and moreover the stability parameter $\zeta_h$ is not defined in ice situations. The stability parameter $\zeta_h$ was derived from $\overline{Ri}_s$ by using the relationships between $Ri$ and $z/L_*$ given by Pruitt et al. (1973). The values of the universal similarity functions $A_h$ and $B_h$ agree closely with the other determinations of these functions and the trend with stability also agrees with that shown in other studies (Arya 1975a; Wippermann 1972c; Melgarejo & Deardorff 1974; Zilitinkevich 1975). Third-degree polynomials fitted to these empirical points, as in Arya (1975a), give the interpolated values of $A_h$ and $B_h$ for adiabatic conditions:

$$A_h = 2.2 \; ; \; B_h = 4.9$$

They fall within the general range of variation of these constants, but since the scatter is tremendous (see e.g. Wippermann, 1970), it seems useless to discuss the reliability of our results.

Yordanov & Wippermann (1972) have shown that baroclinicity can be included in these resistance laws without changing their form but at the cost that the new universal functions $A_i$ and $B_i$ depend now on 2 additional parameters. Moreover, for practical reasons the surface geostrophic wind is used instead of the barotropic constant geostrophic wind. Thus, we have:

$$\frac{U_{g0}}{u_*} = \frac{1}{\kappa}\left[\ln(h/z_0) - A_i(\zeta_h, \mu_h, S_x, S_y)\right] \tag{40a}$$

$$\frac{V_{g0}}{u_*} = -\frac{1}{\kappa} B_i(\zeta_h, \mu_h, S_x, S_y) \tag{40b}$$

where the two parameters $S_x$ and $S_y$ were defined in (30).

The main problem is of course to express the individual effects of these four parameters within $A_i$ and $B_i$. In Arya & Wyngaard (1975), an expression for these functions was derived from some simple arguments relating to the equality of mass flow

in barotropic and baroclinic conditions. An interesting feature of this result is that the functions are decomposed into their barotropic and baroclinic components, i.e.:

$$A_i(\zeta_h, \mu_h, S_x, S_y) = A_h(\zeta_h, \mu_h) + \tfrac{1}{2}\kappa S_x \tag{41a}$$

$$B_i(\zeta_h, \mu_h, S_x, S_y) = B_h(\zeta_h, \mu_h) + \tfrac{1}{2}\kappa S_y \tag{41b}$$

Thus, the functions $A_i$ and $B_i$ may be computed from equations (40) and substitution of their values in (41) permits the calculation of $A_h$ and $B_h$ with the baroclinic effects eliminated. These new values of $A_h$ and $B_h$ may be expected to show a smaller scatter than those given in Table 12. The results of these calculations are reported in Table 13. The variation of these universal functions with the stability parameter $\zeta_h$ was once again fitted with third-degree polynomials. The regression curves and the empirical points are plotted in Fig. 25. The elimination of baroclinicity has slightly reduced the scatter of the points and the agreement with the polynomial regression curves is better (decrease of the standard error of estimate, increase of the multiple correlation coefficient).

TABLE 13. Values of the universal similarity functions including the effect of baroclinicity. The different quantities in the Table are related through eqs. (41).

| Groups | | N | $\zeta_h$ | $\frac{1}{2}KS_x$ | $\frac{1}{2}KS_y$ | $A_i$ | $B_i$ | $A_h$ | $B_h$ |
|---|---|---|---|---|---|---|---|---|---|
| stable ..... | 171°—240° | 26 | 30.9 | —0.50 | —1.19 | —3.73 | 10.19 | —3.23 | 11.38 |
| | 241°—290° | 24 | 31.3 | —0.26 | —0.14 | 1.47 | 10.18 | 1.73 | 10.32 |
| | 291°—360° | 15 | 7.3 | 0.31 | —0.08 | —2.26 | 5.23 | —2.57 | 5.31 |
| unstable .... | 0°—80 ° | 43 | —91.6 | —0.25 | 1.07 | 7.89 | 3.43 | 8.14 | 2.36 |
| | 110°—170° | 7 | —24.5 | 0.09 | —0.35 | 6.15 | 2.32 | 6.06 | 2.67 |
| | 171°—240° | 11 | —35.2 | 0.35 | —0.73 | —0.23 | 3.34 | —0.58 | 4.07 |
| | 241°—290° | 16 | —13.6 | —0.61 | —0.84 | 4.94 | 2.35 | 5.55 | 3.19 |
| | 291°—360° | 38 | —38.0 | 0.96 | —0.81 | —0.02 | 0.6 | —0.98 | 1.41 |

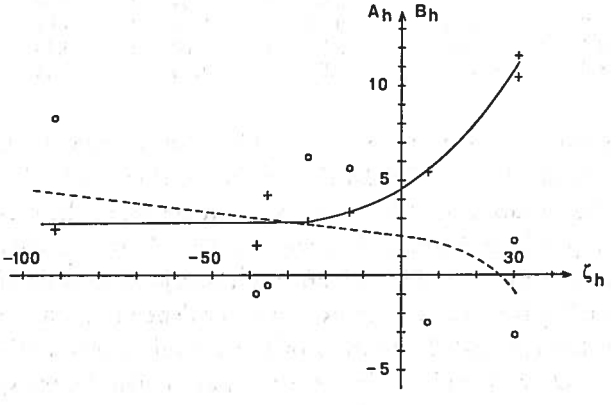


Fig. 25. Variations of the similarity functions $A_h$ (open circles) and $B_h$ (crosses) with stability ($\zeta_h$). The curves are third-degree polynomials fitted to each distribution: $A_h$, dashed line; $B_h$, solid line.

One notices that the function $B_h$ is surprisingly well defined by the empirical points, whereas the function $A_h$ has a large scatter. Interpolation of the neutral values now gives:

$$A_h = 1.92 \; ; \; B_h = 4.54$$

Arya & Wyngaard (1975) have also expressed the functions $A_i$ and $B_i$ for a baroclinic planetary boundary layer, but in the special case of a convective situation. By using the fact that actual wind shear is negligible owing to strong mixing, they obtain the following expression for the universal functions $A_h$ and $B_h$:

$$A_{hi} = \ln (h/z_0) - \kappa \frac{U}{u_*} \approx \ln(-\zeta_h) + C \qquad (42a)$$

$$B_{hi} = \kappa \frac{u_*}{fh} \qquad (42b)$$

where $C$ is a constant depending only on the height of the surface shear layer, and these approximations being valid for $-\zeta_h \geq 10$. This simple model was applied to our 5 sets of data corresponding to unstable conditions. The results are given in Table 14, which shows that this model underestimates the values of $A_h$, but this may be due to the choice of the constant $C$ (Arya & Wyngaard took $C = 0$) since the departure from the model appears to be independent of $\zeta_h$, except for two of our values showing no correlation at all (groups 171°—240° and 291°—360°). As to the function $B_h$, the agreement is best for the two directional groups expected to have the most unstable conditions (groups 0°—80° and 291°—360°).

TABLE 14. Comparison of our similarity functions $A_h$ and $B_h$ with those obtained from a convective planetary boundary layer model.

| Groups | | $\zeta_h$ | $A_{hi}$ | $A_h$ | $B_{hi}$ | $B_h$ |
|---|---|---|---|---|---|---|
| unstable .... | 0°—80° | —91.6 | 4.52 | 8.14 | 2.50 | 2.36 |
| | 110°—170° | —24.5 | 3.20 | 6.06 | 3.64 | 2.67 |
| | 171°—240° | —35.2 | 3.56 | —0.58 | 1.25 | 4.07 |
| | 241°—290° | —13.6 | 2.61 | 5.55 | 1.60 | 3.19 |
| | 291°—360° | —38.0 | 3.64 | —0.98 | 1.33 | 1.41 |

If we now take the wind velocity at $z = h$ as the geostrophic wind, we can check the resistance laws with our individual data. Fig. 26 shows the veering angle $\Delta\alpha_h$ between the wind direction at the surface and at $h = 500$ m as a function of the stability parameter $Ri_*$. The corresponding theoretical curve based on Wangara data for the derived resistance laws is shown in Fig. 27 after Melgarejo & Deardorff (1974). Their stability parameter $Ri_B$ is a bulk Richardson number depending on the temperature difference between the top and the bottom of the boundary layer. Although our data present a large scatter, there is a fair agreement, even quantitatively,

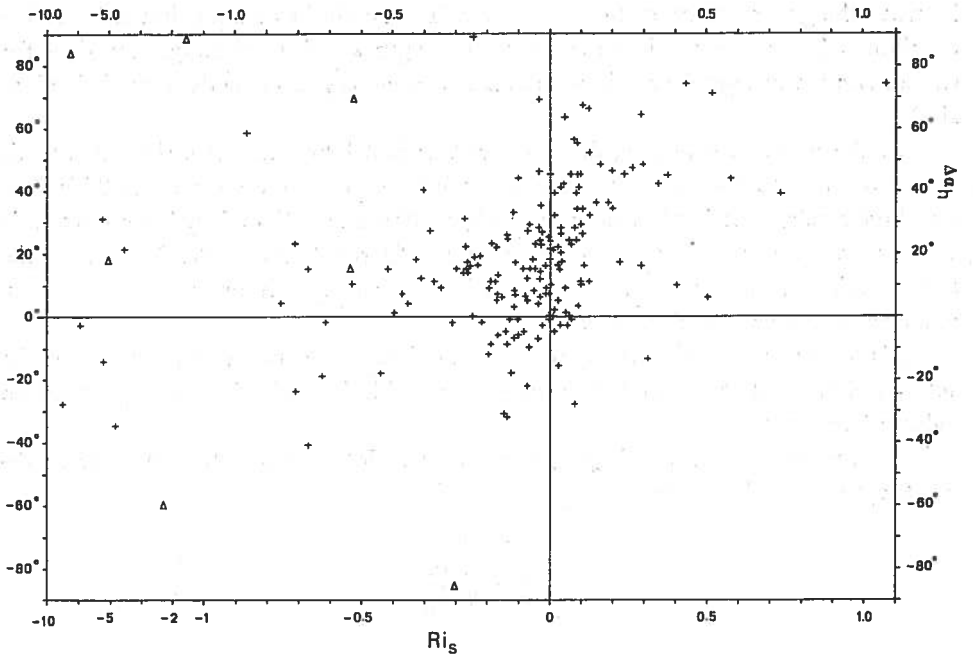


Fig. 26. Distribution of the Utö data for the dependence between the veering angle at h = 500 m and the Richardson number $Ri_s$. The triangles indicate peculiar profiles as defined in connection with Fig. 5. The scale of the abscissa is not continuous for negative $Ri_s$.

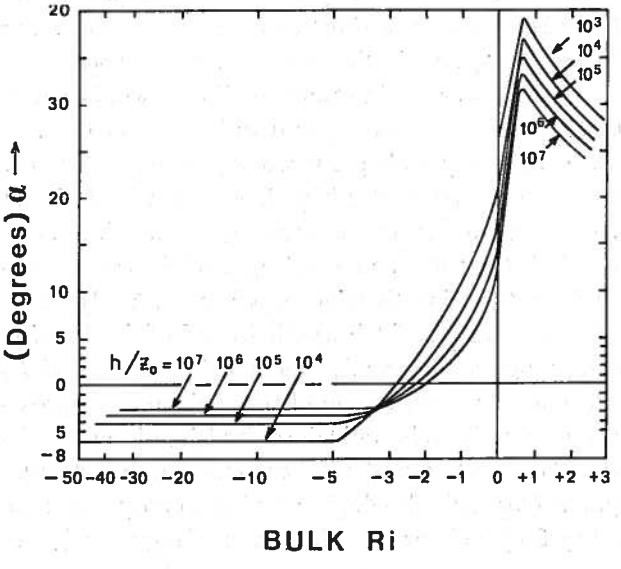


Fig. 27. The angle between the wind direction at the bottom and the top of the boundary layer as a function of a bulk Richardson number and $h/z_0$. The abscissa changes from linear to logarithmic at $Ri_B = -3$. (After Melgarejo & Deardorff, 1974).

between the general trend of the two curves. The angle shows a maximum for stable conditions but seems to decrease for very strong stability, although the data for these cases are meagre (possibly the planetary boundary layer tends towards laminarity).

On the unstable side, $\Delta\alpha_h$ decreases but as instability increases the angle tends asymptotically toward a constant value, which seems to be negative. This is a puzzling result, as it implies no cross-isobaric flow in the boundary layer as a whole to balance the surface-induced frictional force. Clarke & Hess (1974) observed the same tendency. It may be due to air subsidence at $z = h$ or, as we have often mentioned, to baroclinicity effect.

It is very probable that the scatter of our data would be greatly reduced if the actual height h of the boundary layer was available instead of an average constant value of 500 m.

The velocity ratio $R_h = V_s/V_h$ may also be plotted, since the resistance coefficient $u_*/V_h$ may be written:

$$\frac{u_*}{V_h} = \frac{u_*}{V_s}\frac{V_s}{V_h}$$

Our data for $V_s/V_h$ as a function of $Ri_s$ are shown in Fig. 28. The resistance coefficient $u_*/V_h$ obtained from the Wangara data by Melgarejo & Deardorff (1974) is presented in Fig. 29. On the unstable side, the coefficient is strongly dependent on the parameter $h/z_0$, which explains the scatter of our points. However, the two curves show qualitative agreement, especially on the stable side, where the empirical points tend to collapse to one single curve as it is theoretically predicted. The quantitative correspondence may also be checked through the estimation of the ratio $u_*/V_s$. Our grouped data give a mean value of $3.1 \times 10^{-2}$ in the two most stable cases.
Then, the rather constant value of $V_s/V_h \approx 0.5$ in stable conditions would correspond to a value of $u_*/V_h \approx 0.015$, which may be compared with the value 0.007 of Fig. 29. On the unstable side the scatter is quite large. It would, of course, be very interesting to explain this scatter with the parameter $h/z_0$. Unfortunately, $z_0$ is not available for individual data. However, since $z_0$ is a measure of the roughness elements of the surface, it can be assimilated with the mean height of the surface seawaves $h_s$ in a well-developed turbulent motion (Kitaigorodskii et al., 1973). In its turn, $h_s$ is a function of the surface wind, of the fetch length $L_f$ and of the duration of the forcing effect. There are nomograms giving $h_s$ as a function of $V_s$ and $L_f$ (e.g. Bretschneider 1973), and when $h_s$ is known, we can obtain $z_0$ from the approximate relation $z_0 \approx h_s/30$. Unfortunately, the values obtained for $h/z_0$ did not fit the scattered distribution of the ratio $R_h$. Apart from the inaccuracies and uncertainties contained in the above assumptions (e.g. only developing surface gravity waves are predicted by the nomograms, they forget about the effect of standing waves), one

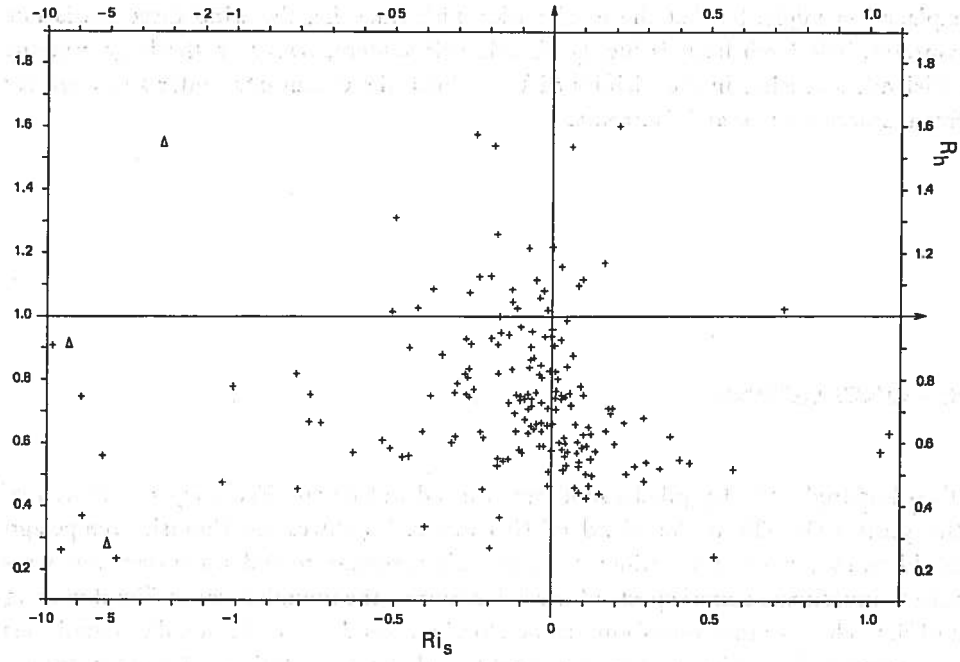


Fig. 28. Distribution of the Utö data for the dependence between the ratio $R_h$ at h = 500 m and the stability parameter $Ri_s$. See caption of Fig. 26.

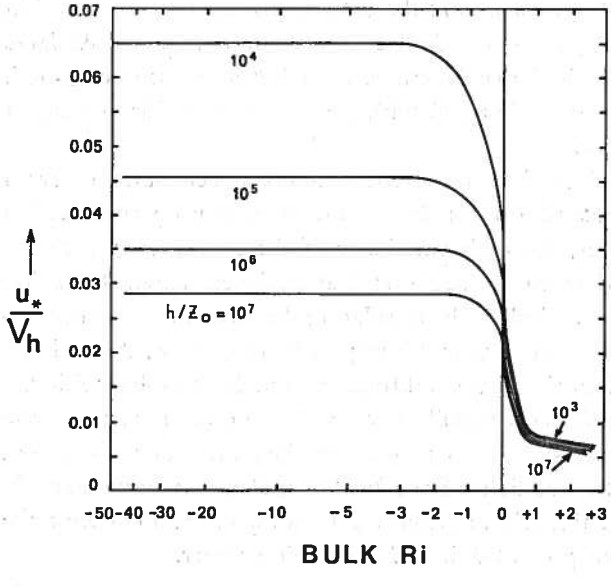


Fig. 29. The resistance coefficient $u_*/V_h$ as a function of a bulk Richardson number $Ri_B$ and $h/z_0$. The absissa changes from linear to logarithmic at $Ri_B = -3$. (After Melgarejo & Deardorff, 1974).

explanation might be that the fetch varies with time, i.e. the wind direction is not constant. The fetch itself is highly direction-dependent, owing to the large amount of islands and islets in the vicinity of Utö. Thus, the conditions under study are far from homogeneous and isotropic.

## 8. CONCLUSIONS

Two hundred and fifty pibal soundings, carried out during February and March of the years 1930—36 at the island of Utö in the Southwestern Finnish archipelago could be used with observations of surface air temperature and sea surface temperature to investigate some aspects of the behaviour of the boundary layer. Wind veering and the velocity ratio were found to be closely dependent on the stability conditions prevailing at the surface and the values obtained agreed with those of similar studies. Baroclinic effects were assessed from average profiles (stationarity and a simple model of geostrophic wind profiles). The results show that boundary layer parameters, such as the cross-isobar angle, the surface stress and the drag coefficients, are sensitive functions of the orientation of the thermal wind with respect to the air flow. Finally, the similarity theory methodology was applied to the data. The internal parameters yielded the expected dimensionless profiles and the external parameters were used in an attempt to predict the velocity ratio and wind veering from commonly available routine variables. The universal similarity functions $A$ and $B$ were also computed. Their neutral numerical value and their trend with stability was in fair agreement with the results of other studies.

In spite of the limitations of the data, the present results are encouraging from the point of view of the parameterization of the boundary layer properties needed for the ice-drift model. However, the high variability of these properties with the different situations encountered in nature suggests that statistical parameterization will not be enough. Instead, a numerical model simulating the structure and development of the real atmospheric boundary layer with respect to roughness, thermal stability, non-homogeneity and baroclinicity conditions should be coupled with the ice-drift model. Much more empirical data will of course be required for an accurate parameterization of the diverse processes to be included in the model. For this reason, a measurement expedition to the ice field of the Bothnian Bay was undertaken in late winter 1977. The results of this trip are expected to complete and continue the present study, and they will be presented in a forthcoming paper.

**ACKNOWLEDGEMENTS**

I want to express my sincerest thanks to Dr. P. Mälkki, Head of the Department of Physical Oceanography at the Institute of Marine Research, who allowed me complete latitude in the conduction of this study. I am also greatly indebted to Prof. E. Holopainen for his guidance and valuable comments and advice given during the course of the study. My special thanks are due to Prof. S. A. Kitaigorodskii for opening new horizons to me at an early stage of this research. I am also grateful to Dr. J. Riissanen, department head at the Finnish Meteorological Institute, Helsinki, for providing the basic data and to the skill of Mr. S. Pietikäinen in writing computer programs. This research was supported by the Board of Navigation.

REFERENCES

Arya, S. P. S. 1975a: Geostrophic drag and heat transfer relations for the atmospheric boundary layer. — *Quart. J. Roy. Meteor. Soc.* 101 (427): 147—161.

—»— 1975b: A drag partition theory for determining the large-scale roughness parameter and wind stress on the Arctic pack ice. — *J. Geophys. Res.* 80 (24): 3447—3454.

—»— & Wyngaard, J. C. 1975: Effect of baroclinicity on wind profiles and the geostrophic drag law for the convective planetary boundary layer. — *J. Atm. Sci.* 32 (4): 767—778.

Banke, E. G. & Smith, S. D. 1973: Wind stress on Arctic sea ice. — *J. Geophys. Res.* 78 (33): 7871—7883.

—»—, Smith, S. D. & Anderson, R. J. 1976: Recent measurements of wind stress on Arctic sea ice.— *J. Fish. Res. Board Can.* 33 (10): 2307—2317.

Bernstein, A. B. 1973: Some observations of the influence of geostrophic shear on the cross-isobar angle of the surface wind. — *Bound. Layer Meteor.* 3 (3): 381—384.

Blackadar, A. K. & Tennekes, H. 1968: Asymptotic similarity in neutral barotropic planetary boundary layers. — *J. Atmos. Sci.* 25 (6): 1015—1020.

Bretschneider, C. L. 1973: Prediction of waves and currents. — *Look Lab/Hawaii* 3 (1): 1—18.

Brocks, K. & Krügermeyer, L. 1972: The hydrodynamic roughness of the sea surface.—*In: Gordon, A. (ed)., Studies in Physical Oceanography* 1: 75—92. New York.

Brown, P. R. 1953: Wave data for the Eastern North Atlantic. — *Mar. Observer* 23: 94—98.

Businger, J. A. & Arya, S. P. S. 1974: The height of the mixed layer in the stably stratified planetary boundary layer. — *Adv. in Geophys.* 18A: 73—91. New York.

—»— , Wyngaard, J. C., Izumi I. & Bradley, E. F. 1971: Fluxprofile relationships in the atmospheric surface layer. — *J. Atmos. Sci.* 28 (2): 181—189.

Campbell, W. J. 1965: The wind driven circulation of ice and water in a Polar Ocean. —*J. Geophys. Res.* 70 (14): 3279—3301.

Charnock, H. 1955: Wind stress on a water surface.— *Quart. J. Roy. Meteor. Soc.* 81 (350): 639—642.

Clarke, R. H. 1970: Observational studies in the atmospheric boundary layer.— *Quart. J. Roy. Meteor. Soc.* 96 (407): 91—114.

—»—, Dyer, A. J., Brook. R. R., Reid D. G. & Troup, A. J. 1971: The Wangara Experiment: boundary layer data. — *CSIRO, Div. Met. Phys. Techn. Paper* 19: 1—362.

—»—, & Hess, G. D. 1974: Geostrophic departure and the functions A and B of Rossby-number similarity theory. — *Bound. Layer Meteor.* 7 (3): 267—287.

Csanady, G. T. 1967: On the resistance law of a turbulent Ekman layer.— *J. Atmos. Sci.* 24 (5): 467—471.

Darbyshire, J. & Darbyshire, M. 1955: Determination of wind stress on the surface of Lough Neagh by measurement of tilt. — *Quart. J. Roy. Meteor. Soc.* 81 (349): 333—339.

Deacon, E. L. 1973: Geostrophic drag coefficients. — *Bound. Layer Meteor.* 5 (3): 321—340.

Deardorff, J. W. 1970a: Preliminary results from numerical integrations of the unstable planetary boundary layer. — *J. Atmos. Sci.* 27 (8): 1209—1211.

—»— 1970b: Convective velocity and temperature scales for the unstable planetary boundary layer and for Rayleigh convection. — *J. Atmos. Sci.* 27 (8): 1211—1213.

—»— 1972a: Numerical investigation of neutral and unstable planetary boundary layers. — *J. Atmos. Sci.* 29 (1): 91—115.

Findlater, J., Harrower, T. N. S., Howkins, G. A. & Wright, H. L. 1966: Surface and 900 mb wind relationships. — *Meteor. Office Scientific Paper* 23: 1—41. London.

Fleagle, R. G. 1956: Note on the effect of air-sea temperature difference on wave generation.— *Trans. Amer. Geophys. Un.* 37: 275—277.

Frost, R. 1948: Atmospheric turbulence. — *Quart. J. Roy. Meteor. Soc.* 74 (321): 316—338.

Gill, A. E. 1968: Similarity theory and geostrophic adjustment.— *Quart. J. Roy. Meteor. Soc.* 94 (402): 581—585.

Gordon, A. H. 1950: The ratio between observed velocities of the wind at 50 feet and 2000 feet over the North Atlantic Ocean. — *Quart. J. Roy. Meteor. Soc.* 76 (329): 344—348.

Guterman, I. G. & Hanevskoi, I. V. 1963: Aeroclimatological Atlas of the Northern Hemisphere (in Russian). — *Hydrometeorological Publishing House*, Leningrad.

Hasse, L. & Dunckel, M. 1974: Direct determination of geostrophic drag coefficients at sea.—*Bound. Layer Meteor.* 7 (3): 323—329.

—»—, & Wagner, V. 1971: On the relationship between the geostrophic and surface wind at sea.— *Mon. Weath. Rev.* 99 (4): 255—260.

Holopainen, E. 1961: Some empirical stress-values for the lower troposphere.— *Geophysica* 8 (2): 151—157.

Hoxit, L. R. 1974: Planetary boundary layer winds in baroclinic conditions.— *J. Atmos. Sci.* 31 (4): 1003—1020.

Hsu, S. A. 1974: On the log-linear wind profile and the relationship between shear stress and stability characteristics over the sea. — *Bound. Layer Meteor.* 6 (3/4): 508—514.

Joffre, S. M. 1975: Ice roughness parameters. — 8 pp. (*Manuscript, Inst. Marine Res.*, Helsinki.)

Johnson, W. B. Jr 1962: Climatology of atmospheric boundary layer parameters and energy dissipation, derived from Gregg's aerological survey of the U.S. — *In: Studies of the three-dimensional structure of the planetary boundary layer, Final Report, Univ. of Wisconsin, Dept. of Meteor.*: 125—158.

Kaimal, J. C., Wyngaard, J. C., Haugen, D. A., Coté, O. R., Izumi, Y., Caughey, S. J. & Readings, C. J. 1976: Turbulence structure in the convective boundary layer. — *J. Atmos. Sci.* 33 (11): 2152—2169.

Kazanski, A. B. & Monin, A. S. 1960: A turbulent regime above the ground atmospheric layer.— *Izv. Akad. Nauk SSSR, Ser. Geofiz.* 1: 165—168.

Kitaigorodskii, S. A. 1969: Small-scale atmosphere-ocean interactions. — *Izv. Atmos. Ocean. Phys.* 5 (11): 641—650.

—»— & Joffre, S. M. 1976: A lecture course on the atmospheric boundary layer.— *Dept. of Meteor., Univ. of Helsinki.* - 207 pp.

—»— , Kuznetsov, O. A. & Panin, G. N. 1973: Coefficients of drag, sensible heat and evaporation in the atmosphere over the surface of the sea. — *Izv. Atmos. Ocean. Phys.* 9 (11): 644—647.

Kolkki, O. 1969: Katsaus Suomen ilmastoon. — *Ilmatieteen Laitoksen Tiedonantoja* 18: 1—64.

Lenz, W. 1971: Monatskarten der Temperatur der Ostsee. — *Ergänzungsheft zur deutschen hydrographischen Zeitschrift, Reihe B* (4) 11: 1—148.

Lettau, H. H. 1957: Windprofil, innere Reibung und Energieumsatz in den unteren 500 m über dem Meer. — *Beitr. Phys. Atmos.* 30 (1): 78—96.

—»— 1959: Wind profile, surface stress and geostrophic drag coefficients in the atmospheric surface layer. — *Adv. in Geophys.* 6: 241—257.

—»— 1962: [Unpublished lecture notes]. — Dept. of Meteor., Univ. of Wisconsin.

—»— & Davidson, B. 1958: Exploring the atmosphere's first mile. *I—II*, London.

—»— & Hoeber, H. 1964: Über die Bestimmung der Höhenverteilung von Schubspannung und Austauschkoeffizient in der atmosphärischen Reibungsschicht. — *Beitr. Phys. Atmos.* 37 (2): 105—118.

Melgarejo, J. W. & Deardorff, J. W. 1974: Stability functions for the boundary layer resistance laws bases upon observed boundary layer heights. — *J. Atmos. Sci.* 31 (5): 1324—1333.

Mendenhall, B. R. 1967: A statistical study of frictional wind veering in the planetary boundary layer. — *Atmos. Sci. Paper* 116: 1—57.

Monin, A. S. 1965: Structure of an atmospheric boundary layer. — *Izv. Atmos. Ocean. Phys.* 1 (3): 258—265.

Pruitt, W. O., Morgan, D. L. & Lourence, F. J. 1973: Momentum and mass transfers in the surface boundary layer. — *Quart. J. Roy. Meteor. Soc.* 99 (420) 370—386.

Roll, H. U. 1952: Über Grössenunterschiede der Meereswellen bei Warm- und Kaltluft.— *Dt. hydrogr. Z.* 5 (2): 111—114.

—»— 1965: Physics of the marine atmosphere. — *In: Van Mieghem (ed.), International Geophysics Series.* - 426 pp. New York.

Sheppard, P. A., Charnock, H. & Francis, J. R. D. 1952: Observations of the westerlies over the sea. — *Quart. J. Roy. Meteor. Soc.* 78 (338): 563—582.

Smith, S. D. & Banke E. G. 1975: Variation of the sea surface drag coefficient with speed.— *Quart. J. Roy. Meteor. Soc.* 101 (429): 665—673.

—»—, Banke, E. G. & Johannesen, O. M. 1970: Wind stress and turbulence over ice in the Gulf of St. Lawrence. — *J. Geophys. Res.* 75 (15): 2803—2812.

Sundararajan, A. 1975: Mean Reynolds stress modeling of the atmospheric boundary layer. — 218 pp. (*Ph. D. Dissertation, Univ. of Washington.*)

Tabata, T. 1975: Ice study in the Gulf of Bothnia.— *Low Temperature Science, Ser. A* 33: 191—198 *(in Japanese with English summary).*

Thompson, R. O. R. Y. 1974: The influence of geostrophic shear on the cross-isobar angle of the surface wind. — *Bound. Layer Meteor.* 6 (3/4): 515—518.

Valli, A. & Leppäranta, M. 1975: Calculation of ice drift in the Bothnian Bay and the Quark.—*Styrelsen för Vintersjöfartsforskning, Forskningsrapport* 13: 1—14.

Venho, S. N. 1963: Tuulioloista Suomen rannikkoalueilla.— *Ilmatieteellisen Keskuslaitoksen Tiedonantoja* 3: 1—26.

Weeks, W. F. & Lee, O. S. 1958: Observations on the physical properties of sea-ice at Hopealde, Labrador. — *Arctic* 11 (3): 135—155.

Weller, G. 1968: Heat-energy transfer through a four-layer system: air, snow, sea ice, sea water.— *J. Geophys. Res.* 73 (4): 1209—1220.

Wippermann, F. 1970: The two constants in the resistance law for a neutral barotropic boundary layer of the atmosphere. — *Beitr. Phys. Atmos.* 43 (2): 133—140.

—»— 1972a: Baroclinic effects on the resistance laws for the planetary boundary layer of the atmosphere. — *Beitr. Phys. Atmos.* 45 (3): 244—259.

—»— 1972b: A note on the parameterization of the large-scale wind stress at the sea-surface.— *Beitr. Phys. Atmos.* 45 (3): 260—266.

—»— 1972c: Empirical formulae for the universal functions $M_m(\mu)$ and N $(\mu)$ in the resistance law for a barotropic and diabatic planetary boundary layer. — *Beitr. Phys. Atmos.* 45 (4): 305—311.

Wyngaard, J. C., Arya, S. P. S. & Coté, O. R. 1974: Some aspects of the structure of convective planetary boundary layers. — *J. Atmos. Sci.* 31 (3): 747—754.

Yaglom, A. M. 1977: Comments on wind and temperature flux-profile relationships. — *Bound. Layer Meteor.* 11 (1): 89—102.

Yordanov, D. & Wippermann, F. 1972: The parameterization of the turbulent fluxes of momentum, heat and moisture at the ground in a baroclinic planetary boundary layer. — *Beitr. Phys. Atmos.* 45 (1): 58—65.

Zilitinkevich, S. S. 1972: On the determination of the height of the Ekman boundary layer.— *Bound. Layer Meteor.* 3 (2). 141—145.

—»— 1975: Resistance laws and prediction equations for the depth of the planetary boundary layer. — *J. Atmos. Sci.* 32 (3): 741—752.

—»— & Chalikov, D. V. 1968: The laws of resistance and of heat and moisture exchange in the interaction between the atmosphere and an underlying surface. — *Izv. Atmos. Ocean .Phys.* 4 (7): 438—441.

Zubov, N. N. 1943: Arctic Ice.— *Izdatel'stvo Glavsevmorputi, Moscow (Transl. for AFCRC by USN Oceanographic Office and American Meteorological Society).* - 360 pp.

Merentutkimuslait. julk./Havsforskningsinst. Skr. No. 243 (1978) 63—76.

# INTERCALIBRATION OF METHODS FOR CHLOROPHYLL MEASUREMENTS APPLIED IN THE BALTIC SEA

U. Larsson,[1]) L. Norling,[2]) S. Carlberg,[3]) S. Lööf,[3]) A. Tolstoy,[4]) K. von Bröckel,[5]) V. Elizarjeva,[6]) W. Kaiser,[7]) J. Lassig[8]) T. Melvasalo,[9]) I. Mäkinen,[9])

Abstract

Two meetings were arranged, in 1974 and 1975, under the auspices of the Baltic Sea Expert Meeting on Intercalibration of Biological and Chemical Methods, to intercalibrate methods for the measurement of chlorophylls. The only analyses yielding values of acceptable precision were those made for chlorophyll *a* according to Strickland & Parsons (1968) and SCOR-Unesco (1966). All the other analyses yielded more or less scattered values, with rather high coefficients of variation for the participating laboratories. In the 1974 intercalibration almost all the results were different at the 5 or 1 % significance level. In 1975 the chlorophyll *a* measurements of all the participating laboratories were in good agreement, which indicates that at least this parameter could be measured with sufficient accuracy. The results show clearly that careful and standardized handling of the samples is essential for comparable and reproducible results. This is of the utmost importance with measurements carried out in, for example, monitoring studies involving several laboratories.

1. Department of Zoology and the Askö Laboratory, University of Stockholm, P.O. Box 6801, S-113 86 Stockholm, Sweden.
2. National Swedish Environment Protection Board, Fack S-171 20 Solna, Sweden.
3. Fishery Board of Sweden, Hydrographical department, Fack S-413 10 Göteborg, Sweden.
4. National Swedish Environment Protection Board, Limnological Survey, Box 557, S-751 22 Uppsala, Sweden.
5. Institut für Meereskunde an der Universität Kiel, Düsternbrooker Weg 20, 23 Kiel, FRG.
6. Institute of Biology of Internal Waters of the Academy of Science of the USSR.
7. Institut für Meereskunde der Akademie der Wissenschaften der DDR, Seestrasse 15, DDR-253 Warnemünde, DDR.
8. Institute of Marine Research, P.O. Box 166, SF-00141 Helsinki 14, Finland.
9. National Board of Waters, Water Research Laboratory, P.O. Box 250, SF-00101 Helsinki 10, Finland.

## INTRODUCTION

The growing interest in the Baltic as a natural resource threatened by pollution has called attention to the need for a system of monitoring parameters that will give comparable results for all the laboratories working in the Baltic.

A basic need in any aquatic ecosystem monitoring programme is some parameter which can serve as a measure of phytoplankton biomass. Perhaps the most widely used, and also the least time-consuming, solution is to measure the amount of chlorophyll in the phytoplankton. However, the extraction and measurement of chlorophyll is a process with several steps, each of which can be performed in several at least slightly different ways, and it is further complicated by the presence of different types of chlorophylls (*a*, *b*, *c*) and of pheo-pigments, breakdown products of the chlorophylls, with similar absorption peaks in spectrophotometric analysis. These complications make it obvious that intercalibration is necessary before two different methods of measuring chlorophyll can be assumed to give comparable results.

The present paper reports the results from two such intercalibrations concerning the measurement of chlorophylls and pheo-pigments, made during two Baltic Sea Expert Meetings on Intercalibration of Biological and Chemical Methods, sponsored by the National Swedish Environment Protection Board.

The objective of the meetings was to investigate the comparability of the methods used, and to establish standardized procedures for use in monitoring programmes in the Baltic. The work was not directed to the development of new methods, but was intended merely to synthesize the already existing »know how» into an acceptable method, to be recommended for use in monitoring studies in the Baltic.

The two meetings were held at the Askö Laboratory on June 8—15, 1974 and on July 6—12, 1975. The laboratories represented at the first meeting were those of Institut für Meereskunde der Akademie der Wissenschaften der DDR (AW. GDR), the Institute of Marine Research, Finland (IMR. Fin.), the National Board of Waters, Finland (NBW. Fin.), Institut für Meereskunde an der Universität Kiel, FRG (IFM. FRG), the Fishery Board of Sweden, Hydrographical Department (FBS. Swe.), the National Swedish Environment Protection Board, Limnological Survey, (LS. Swe.), and the Askö Laboratory, Sweden (AL. Swe.). In the second meeting only the above mentioned Swedish laboratories participated, together with one USSR laboratory, that of the Hydrometeorological Service of the USSR (HS. USSR).

The aim of the first intercalibration was not to examine all the problems involved in the measurement of chlorophylls and their derivatives, but merely to obtain a general idea of the comparability of the different methods applied within the Baltic countries. The results of this first meeting clearly indicated the need for a more detailed study of the methods, aimed at revealing the main causes of the discrepancies.

Such a study and an intercalibration with one USSR laboratory, was made by the Swedish laboratories during the 1975 meeting (the results of this detailed study are reported in a separate paper).

## MAIN FEATURES OF THE METHODS USED

The Institute of Marine Research, Finland, used a calibrated fluorometer (as described in Strickland & Parsons, 1968). All the other laboratories used spectrophotometric methods as described in Lorenzen (1967), Strickland & Parsons (1968) and SCOR-Unesco, Working Group 17 (1966).

In each laboratory, however, the procedure used was modified to a greater or lesser extent; the main features of the modified versions are listed in Table 1.

## EXPERIMENTAL DESIGN

Each participating laboratory took ten replicate samples from a large tank, in which the water was continuously mixed during sampling. The tank was first filled with water from an unpolluted area and later with water from a highly eutrophicated area. In 1974, the samples were then treated as described for each laboratory (Table 1). In 1975, two litres of water were strained through each of a series of filters, using the same filtering equipment. All the filters were furnished with 3 ml of a magnesium (hydroxy) carbonate suspension, before filtering. The filters were dried in an airstream of room temperature and randomly put together in groups of ten. Each group of filters was deep-frozen to —20°C in an airtight container containing silica gel, and distributed deep-frozen to the laboratories. The analyses were carried out after eight weeks in the respective laboratories.

## STATISTICAL CALCULATIONS

The data were treated on the assumption that they were normally distributed. For each laboratory and parameter the mean value, the standard deviation and the confidence interval (95 %) were calculated.

The difference between mean values was tested with the t-test, assuming normal distribution and common standard deviations.

In some cases it was obvious that the mean values were significantly different and thus no t-tests were performed. In other cases it was clear that the assumption of common variances was invalid. Despite this, t-tests were performed because the number of observations were the same. In multiple t-tests performed on samples from different populations with the same null hypothesis, the significance level is reduced. In most cases, however, the t-values obtained were so large that it was obvious that the 5 % significance level was reached.

# RESULTS

The results from the intercalibrations are presented in Tables 2—4. Table 5 shows the degree of significance of the differences between all possible pairs tested. For both sets of measurements made in 1974 it is obvious that the comparability of the measurements is rather low. The tests which showed no significant differences between the mean values are rather uncertain as this could be expected to occur randomly in a material with no consistent trend for any tested pair of values.

Tables 2—4 also show that the trend toward high or low values compared to the grand mean is consistent for each laboratory throughout the two series of measurements in 1974 (the only noteworthy exception is the AL. Swe. for pheo-pigments).

It is obvious from the coefficients of variation (if a value of 10 % is accepted as a maximum value, see Discussion) presented in Table 6, that the reproducibility of the measurements within each laboratory is acceptable only for chlorophyll *a* (according to Strickland & Parsons, 1968, and SCOR-Unesco, 1966 and in some cases also according to Lorenzen, 1967).

In the 1975 intercalibration the very large discrepancies which occurred in the measurements from 1974 (to some extent depending on analytical failures which will be discussed later) had almost disappeared. Exceptions are the measurements from the USSR laboratory for chlorophyll *a* and pheo-pigments (Lorenzen 1967) and the AL. Swe. for pheo-pigments. With regard to the reproducibility of the measurements, as indicated by the coefficient of variation, Table 6, the results in 1975 were generally in good agreement with those from 1974.

The deviations from the grand mean (laboratories participating in both 1974 and 1975), Tables 2—4, were in the same direction in 1975, except for the AL. Swe. (chl *b*) and LS. Swe. (pheop.). This together with the relatively good reproducibility for those laboratories participating in both intercalibrations suggests that the errors affecting the comparability of the measurements are of a systematic character.

The algal composition (only the dominant species) on the various sampling occasions is shown in Table 7 A together with the main chlorophylls occurring in these groups (Table 7 B).

## DISCUSSION

It is obvious when the results from 1974 are compared with those from 1975 that there have been large improvements among the Swedish laboratories, especially for chlorophyll *a* according to Strickland & Parsons (1968) and SCOR-Unesco (1966), but also for chlorophyll *a* according to Lorenzen (1967). These results should, however, be regarded with some caution as part of the analytical procedure wasexcluded (see Experimental design), which may have eliminated analytical errors, as for example in the storage of sampled water, choice of filter type, filtering procedure and preservation of filters (Larsson et al. in prep.). Minor changes in the analytical procedures, towards greater uniformity among the Swedish laboratories, were carried out in the 1975 intercalibration (Table 1), and some of these may have affected the final results, which stresses the importance of standardizing procedures.

Some of the strongly deviating results in the 1974 intercalibration may have been caused by the unfamiliarity of the workers with the conditions and levels of concentrations in the water (NBW. Fin. filtered too small a volume of water to obtain reliable results. The filters were also stored for a longer time than those of the other laboratories. FBS. Swe. used cellulose acetate filters, which became clogged with the high

content of particulate matter in the water on June 12, 1974) or unreliable instruments (Al. Swe. used a spectrophotometer which, when compared with other instruments, was found to yield erroneous results). There was no opportunity adequately to investigate the influence of variation in the phytoplankton composition upon the results. In 1974 the drastic difference in phytoplankton composition between the two intercalibrations did not seem to affect the internal relationships among the participating laboratories. However, this may merely indicate that the change in the quantitative extraction of chlorophylls was not so great that it could be distinguished in these results. There is evidence in the literature of considerable interspecific differences in the extractability of chlorophylls (SCOR-Unesco 1966), which suggests that this might not only cause errors in the absolute quantitative estimates, but also affect the comparability between different laboratories when different extraction methods are used.

A major problem in intercalibrations of biological parameters is that it is very difficult or impossible to determine the »true value» of the parameter measured (SCOR-Unesco 1966). (It must be remembered here that the »grand mean» should not be regarded as anything but a tool for the interpretation of the data). Combined with the lack of data in the literature on the reproducibility of the methods, especially when applied on a routine basis, this constitutes a major uncertainty in the interpretation of the results. Calculations made by Ryding (1975), and Tett et al. (1975), the latter on the basis of literature data, indicate that a coefficient of variation of about 10 % is reasonable for chlorophyll *a* measurements according to both Strickland & Parsons (1968) and Lorenzen (1967). This value is also in good agreement with the results presented in this paper (Table 6). It is therefore suggested that in the measurement of chlorophyll *a* the coefficient of variation should not be higher than about 10 % for the precision of the results to be acceptable. The precision of the measurements of the remaining pigments is obviously much lower. It is a well-known fact that the accuracy of measurements is dependent both on the pigments and on their concentration (Strickland & Parsons 1968, Lorenzen 1967). The precision of the absorbance measurements decreases towards low (and high) absorbance values (Kolthoff & Sandell 1956). This, in combination with the different magnitudes of the constants (chl *a*: 11.6, chl *b*: 20.5 and chl *c*: 55) in the calculation formulas used, magnifies the errors in the calculated concentrations, which increase in the order chl *a*, chl *b*, chl *c*. Thus the determination of chl *b* and *c* becomes uncertain, and must be regarded more as a qualitative than a quantitative description of the phytoplankton population. The same seems to be valid for the measurements of pheo-pigment *a*. The very poor precision of chl *c* readings was pointed out by Strickland & Parsons (1968), who also noted that the recovery of chl *c* was almost always higher than the added amounts. Later determinations of the constants by Jeffrey & Humphrey (1975) have shown that the extinction coefficient for chl *c* should be approximately twice the value used earlier, which in practice means that the new equations will yield only half the amount given by the old ones.

It is obvious from this work that even the measurement of chlorophylls, which has been considered very simple and has therefore been widely applied in both ecological and monitoring studies, demands careful and standardized handling to yield reproducible and comparable results. Every step in the analysis involves a possible source of error (some of these sources of error have been investigated by Larsson, Carlberg, Lööf and Tolstoy and will be presented elsewhere) which makes it essential to use standardized methods, especially for monitoring studies.

## CONCLUSIONS

1. The only measurements whose precision was acceptable were those obtained for chlorophyll *a* according to Strickland & Parsons (1968) and SCOR-Unesco 1966), and to some extent according to Lorenzen (1967). The measurements of all the other pigments failed to reach an acceptable level of precision.
2. Although the measurement of chlorophyll has been regarded as a simple analytical proeedure, it demands careful management and the appropriate equipment.
3. To obtain comparable results, further standardization is recommended for the methods used in the Baltic Sea Area. This is of special importance for future monitoring programmes.
4. The accuracy of chlorophyll measurements should always be checked with occasional replicate analyses.

**Acknowledgements**

We thank Dr. Ragnar Elmgren for valuable and constructive critizism of the manuscript. Mrs Anna A. Damström, M. A., has revised the English. We are also very grateful to Mrs Kerstin Ernqvist for typing it. The work was supported by the Swedish Environmental Protection Board.

REFERENCES

Derenbach, J. 1969: Zur Homogenisation des Phytoplanktons für die Chlorophyllbestimmung. — *Kieler Meeresforsch.* 25 (1): 166—171.

Jeffrey, S. W. & Humphrey, G. F. 1975: New spectrophotometric equations for determining chlorophylls *a*, *b*, *c*, and $c_2$ in higher plants, algae and natural phytoplankton. — *Biochem. Physiol. Pflanzen* (*BPP*) 167: 191—194.

Kolthoff, I. M. & Sandell, E. B. 1956: Textbook of quantitative inorganic analysis. — 759 pp. New York.

Lorenzen, C. J. 1967: Determination of chlorophyll and pheo-pigments: Spectrophotometric equations. — *Limnol. Oceanogr.* 12 (2): 343—346.

Ryding, S.-O. 1975: Intercalibration of methods for determining chlorophyll *a* in water. — *Vatten* 31 (4): 327—332.

SCOR-Unesco 1966: Determination of photosynthetic pigments in seawater. — *Monographs on Oceanographic Methodology* 1: 1—69.

Strickland, J. D. M. & Parsons, T. R. 1968: A practical handbook of sea-water analysis. — *Bull. Fish. Res. Board Can.* 167: 1—311.

Tett, P., Kelly, M. G. & Hornberger, G. M. 1975: A method for the spectrophotometric measurement of chlorophyll *a* and pheophytin *a* in benthic microalgae. — *Limnol. Oceanogr.* 20 (5): 887—896.

TABLE 1. Details of methods of participating laboratories.

| Laboratory | Preservation of the sampled water. $MgCO_3$ 1g/100 ml $H_2O$ | Filtration of the water sample | Type of filter | Drying of filter | Vacuum pressure | Storage | Homogenization | Solvent |
|---|---|---|---|---|---|---|---|---|
| Askö Laboratory, Sweden | 3 ml/l[x] | No[x] | Whatman GF/C | No | 0.3 kp·cm$^{-2}$ | Max. 5 weeks —20°C | Teflon pestle | 90 % acetone |
| Fishery Board, Sweden | 1 ml/l | No | Sartorius SM 11306 (1974) Whatman GF/C (1975) | Yes | 0.5 kp·cm$^{-2}$ | Max. 8 weeks —20°C | No[x] | 90 % acetone |
| Inst. of Mar. Res., Finland | 1 ml/l[x] | No[x] | Whatman GF/C | No | 0.5 kp·cm$^{-2}$ | No | Teflon pestle | 90 % acetone |
| Inst. für Meereskunde, GDR | No[x] | No[x] | Schleicher & Schüll No 6[x] | Yes[x] | 0.3 kp·cm$^{-2}$ | Max. 12 weeks 2—4°C[x] | Shaker[x] | 90 % acetone |
| Inst. für Meereskunde, FRG | No[x] | 300 $\mu$[x] net | Whatman GF/C | No | 0.5 kp·cm$^{-2}$ | Max. 8 weeks —20°C | Method[x] in Derenbach 1969 | 90 % acetone |
| National Board of Waters, Finland | 3 ml/l[x] | 300 $\mu$ net | Whatman GF/C | Yes[x] | ? | Max. 5 weeks —20°C | Teflon pestle | 90 % acetone |
| NLS. Sweden | 3 ml/l[x] | No[x] | Whatman GF/C | Yes[x] | 0.9 kp·cm$^{-2}$ | Max. 8 weeks —20°C | Teflon pestle | 90 % acetone |
| Hydromet. Service, USSR 1975 | ? | ? | ? | ? | ? | ? | Grinding | 90 % acetone |

[x] Deviation from the analytical procedure described in the main reference.

TABLE 1, cont.

| Laboratory | Centrifugation | Filtering of the extract | Photometer | Slit width | Wavelengths | Acid | Cuvette path length | Calculation |
|---|---|---|---|---|---|---|---|---|
| Askö Laboratory, Sweden | 4000 rpm/10 min | No | Beckman DU (1974) Bausch & Lomb Spectronic 710 (1975) | 8 nm | 750, 665, 645, 630, 750a, 665a | 1 N HCl 2 dr. | 5 cm | Strickland & Parsons 1968, Lorenzen 1967 |
| Fishery Board, Sweden | 5000 rpm/20 min | No | Hitachi 139 (1974) Bausch & Lomb Spectronic 700 (1975) | 2 nm 8 nm | 750, 663, 645, 630 665x in 1975 | No | 5 cm | Scor-Unesco 1966 |
| Inst. of Mar. Res., Finland | 3000 rpm/10 min | No | Turner 110 (fluorometer) | — | Excitation 430 nm Excitation 650 nm | 6 N HCl 2 dr. | — | Strickland & Parsons 1968 |
| Inst. für Meereskunde, GDR | 6000 rpm/10 minx | No | Spectrophotometer VSY-2 G | ? | 750, 665, 750a, 665a | 1 N HCl 3 dr. | 5 cm | Lorenzen 1967 |
| Inst. für Meereskunde, FRG | 5500 rpm/15 minx | No | Zeiss, PMQ 111 | 2 nm | 750, 665, 645, 630 | No | 2 cm | Scor-Unesco 1966 |
| National Board of Waters, Finland | 3000 rpm/10 min | Yesx | Hitachi 181 | ? | 750, 665, 645, 630 | No | 1 cm | Strickland & Parsons 1968 |
| NLS. Sweden | 4—5000 rpm/10 min | No | Beckman DB-G | 1 nm | 750, 665, 645, 630, 480, 430, 410, 750a, 665a | 0,1 N HClx 3 dr. | 4 cm | Strickland & Parsons 1968, Lorenzen 1967 |
| Hydromet. Service, USSR 1975 | 9000 rpm/15 minx | ? | ? | ? | 750, 663, 645, 630 | No | 2 cmx | Scor-Unesco 1966 |

TABLE 2. Mean value of 10 measurements in mg.m$^{-3}$ ($\bar{x}$). Standard deviation (s), coefficient of variation (CV %), and deviation from »grand mean» for each laboratory and parameter from the intercalibration carried out on June 10, 1974.

| Laboratory | | Strickland & Parsons (1968) SCOR-Unesco (1966) | | | Lorenzen (1967) | |
|---|---|---|---|---|---|---|
| | | Chl a | Chl b | Chl c | Chl a | pheop. |
| AL. Swe | $\bar{x}$ | 0.63 | 0.09 | 0.56 | 0.34 | 0.47 |
| | s | 0.10 | 0.05 | 0.31 | 0.14 | 0.12 |
| | CV % | 16 | 60 | 55 | 41 | 25 |
| | D | —0.38 | —0.08 | +0.14 | —0.32 | +0.19 |
| LS. Swe | $\bar{x}$ | 1.01 | 0.04 | 0.11 | 0.80 | 0.33 |
| | s | 0.04 | 0.04 | 0.08 | 0.05 | 0.10 |
| | CV % | 4 | 90 | 71 | 7 | 29 |
| | D | ±0 | —0.13 | —0.31 | +0.14 | +0.05 |
| FBS. Swe | $\bar{x}$ | 1.12 | 0.36 | 0.60 | | |
| | s | 0.06 | 0.10 | 0.28 | | |
| | CV % | 6 | 27 | 47 | | |
| | D | +0.11 | +0.19 | +0.18 | | |
| AW. GDR | $\bar{x}$ | | | | 0.60 | 0 |
| | s | | | | 0.16 | |
| | CV % | | | | 27 | |
| | D | | | | —0.06 | —0.28 |
| IMR. Fin | $\bar{x}$ | 1.02 | | | 0.88 | 0.31 |
| | s | 0.05 | | | 0.05 | 0.05 |
| | CV % | 4 | | | 5 | 17 |
| | D | +0.01 | | | +0.22 | +0.03 |
| IFM. FRG | $\bar{x}$ | | | | | |
| | s | | | | | |
| | CV % | | | | | |
| | D | | | | | |
| NBW. Fin | $\bar{x}$ | 1.28 | | | | |
| | s | 0.27 | | | | |
| | CV % | 21 | | | | |
| | D | +0.27 | | | | |
| Grand mean | | 1.01 | 0.17 | 0.42 | 0.66 | 0.28 |
| Mean CV % | | 10 | 59 | 58 | 20 | 24 |

TABLE 3. Mean value of 10 measurements in $mg.m^{-3}$ ($\bar{x}$). Standard deviation (s), coefficient of variation (CV %), and deviation from »grand mean» for each laboratory and parameter from the intercalibration carried out on June 12, 1974.

| Laboratory | | Strickland & Parsons (1968) SCOR-Unesco, (1966) | | | Lorenzen (1967) | |
|---|---|---|---|---|---|---|
| | | Chl a | Chl b | Chl c | Chl a | pheop. |
| AL. Swe | $\bar{x}$ | 4.08 | 0.36 | 3.30 | 4.18 | 0.04 |
| | s | 0.27 | 0.07 | 0.45 | 0.44 | |
| | CV % | 7 | 19 | 14 | 11 | |
| | D | —1.10 | —0.44 | +1.4 | —0.39 | —1.13 |
| LS. Swe | $\bar{x}$ | 5.35 | 0.12 | 0.85 | 4.38 | 1.47 |
| | s | 0.38 | 0.04 | 0.10 | 0.28 | 0.31 |
| | CV % | 7 | 32 | 12 | 6 | 21 |
| | D | +0.17 | —0.68 | —1.05 | —0.19 | +0.30 |
| FBS. Swe | $\bar{x}$ | 6.35 | 1.07 | 1.58 | | |
| | s | 1.14 | 0.38 | 0.65 | | |
| | CV % | 18 | 36 | 41 | | |
| | D | +1.17 | +0.27 | —0.32 | | |
| AW. GDR | $\bar{x}$ | | | | 4.71 | 0.92 |
| | s | | | | 0.41 | 0.18 |
| | CV % | | | | 9 | 19 |
| | D | | | | +0.14 | +0.25 |
| IMR. Fin | $\bar{x}$ | 6.21 | | | 5.02 | 2.23 |
| | s | 0.16 | | | 0.11 | 0.32 |
| | CV % | 3 | | | 2 | 14 |
| | D | +1.03 | | | +0.45 | +1.06 |
| IFM. FRG | $\bar{x}$ | 5.26 | 1.64 | 1.85 | | |
| | s | 0.14 | 0.25 | 0.57 | | |
| | CV % | 3 | 15 | 31 | | |
| | D | +0.08 | +0.84 | —0.05 | | |
| NBW. Fin | $\bar{x}$ | 3.84 | | | | |
| | s | 1.27 | | | | |
| | CV % | 33 | | | | |
| | D | —1.34 | | | | |
| Grand mean | | 5.18 | 0.80 | 1.90 | 4.57 | 1.17 |
| Mean CV % | | 12 | 26 | 25 | 7 | 18 |

TABLE 4. Mean value of 10 measurements in mg.m$^{-3}$ ($\bar{x}$). Standard deviation (s), coefficient of variation (CV %), and deviation from »grand mean» for each laboratory and parameter from the intercalibration carried out on July 9, 1975.

| Laboratory | | Strickland & Parsons (1968) SCOR-Unesco (1966) | | | Lorenzen (1967) | |
|---|---|---|---|---|---|---|
| | | Chl a | Chl b | Chl c | Chl a | pheop. |
| AL. Swe | $\bar{x}$ | 1.66 | 0.48 | 0.74 | 1.50 | 0.33 |
| | s | 0.13 | 0.15 | 0.25 | 0.20 | 0.29 |
| | CV % | 8 | 31 | 32 | 13 | 88 |
| | D | ±0 | +0.18 | +0.21 | —0.02 | —0.02 |
| LS. Swe | $\bar{x}$ | 1.63 | 0.12 | 0.08 | 1.52 | 0.21 |
| | s | 0.10 | 0.02 | 0.04 | 0.08 | 0.05 |
| | CV % | 6 | 17 | 50 | 5 | 24 |
| | D | —0.03 | —0.18 | —0.45 | ±0 | —0.14 |
| FBS. Swe | $\bar{x}$ | 1.62 | 0.31 | 0.68 | 1.43 | 0.30 |
| | s | 0.08 | 0.04 | 0.23 | 0.09 | 0.07 |
| | CV % | 5 | 13 | 34 | 6 | 23 |
| | D | —0.04 | +0.01 | +0.15 | —0.09 | —0.05 |
| HS I. USSR | $\bar{x}$ | 1.70 | 0.27 | 0.60 | 1.42 | 0.60 |
| | s | 0.12 | 0.06 | 0.19 | 0.39 | 0.65 |
| | CV % | 7 | 22 | 32 | 27 | 108 |
| | D | +0.04 | —0.03 | +0.07 | —0.10 | +0.25 |
| HS II. USSR | $\bar{x}$ | 1.68 | 0.33 | 0.55 | 1.72 | 0.31 |
| | s | 0.21 | 0.11 | 0.23 | 0.32 | 0.23 |
| | CV % | 13 | 33 | 42 | 19 | 74 |
| | D | +0.02 | +0.03 | +0.02 | +0.20 | —0.04 |
| Grand mean | | 1.66 | 0.30 | 0.53 | 1.52 | 0.35 |
| Mean CV % | | 8 | 23 | 38 | 14 | 63 |

TABLE 5. Results from the t-tests of the differences between the means. The figures represent the significance level at which the tested means are different. »ns» indicates no significant difference. (I: June 10, 1974, II: June 12, 1974 and III: July 9, 1975).

| Laboratory | | Strickland & Parsons (1968) SCOR-Unesco (1966) | | | | | | | | | Lorenzen (1967) | | | | | |
|---|---|---|---|---|---|---|---|---|---|---|---|---|---|---|---|---|
| | | Chl a | | | Chl b | | | Chl c | | | Chl a | | | pheop. | | |
| | | I | II | III | I | II | III | I | II | III | I | II | III | I | II | III |
| AL. Swe | LS. Swe | 5 | 5 | ns | 5 | 5 | 1 | 5 | 5 | 1 | 5 | ns | ns | ns | 5 | ns |
| | AW. GDR | | | | | | | | | | 5 | 5 | | 5 | 5 | |
| | FBS. Swe | 5 | 5 | ns | 5 | 5 | 1 | 5 | 5 | ns | | | ns | ns | | ns |
| | IMR. Fin | 5 | 5 | | | | | | | | 5 | 5 | | 5 | 5 | |
| | NBW. Fin | 5 | ns | | | | | | | | | | | | | |
| | IFM. FRG | | 5 | | | 1 | | | 5 | | 5 | | | | | |
| | HS I. USSR | | | ns | | | 1 | | | ns | | | ns | | | ns |
| | HS II. USSR | | | ns | | | 5 | | | ns | | | ns | | | ns |
| LS. Swe | AW. GDR | | | | | | | | | | 5 | ns | | 5 | 5 | |
| | FBS. Swe | 5 | 5 | ns | 5 | 5 | 1 | 5 | 5 | 1 | | | 5 | ns | | 1 |
| | IMR. Fin | ns | 5 | | | | | | | | 5 | 5 | | ns | 5 | |
| | NBW. Fin | 5 | 5 | | | | | | | | | | | | | |
| | IFM. FRG | | ns | | | 1 | | | 5 | | | | | | | |
| | HS I. USSR | | | ns | | | 1 | | | 1 | | | ns | | | ns |
| | HS II. USSR | | | ns | | | 1 | | | 1 | | | ns | | | ns |
| AW. GDR | FBS. Swe | | | | | | | | | | | | | | | |
| | IMR. Fin | | | | | | | | | | 5 | 5 | | | 5 | |
| FBS. Swe | IMR. Fin | ns | ns | | | | | | | | | | | | | |
| | NBW. Fin | ns | 5 | | | | | | | | | | | | | |
| | IFM. FRG | | 5 | | | ns | | | ns | | | | | | | |
| | HS I. USSR | | | ns | | | ns | | | ns | | | ns | | | ns |
| | HS II. USSR | | | ns | | | ns | | | ns | | | 1 | | | ns |
| IMR. Fin | NBW. Fin | 5 | 5 | | | | | | | | | | | | | |
| | IFM. FRG | | 5 | | | | | | | | | | | | | |
| HS I. USSR | HS II. USSR | | | ns | | | ns | | | ns | | | ns | | | ns |

TABLE 6. Coefficient of variation (CV %) for each laboratory and parameter at the three intercalibrations. (I = June 10, 1974, II = June 12, 1974, III = July 9, 1975). — indicates negative value.

| Laboratory | Strickland & Parsons (1968) SCOR-Unesco (1966) | | | | | | | | | Lorenzen (1967) | | | | | |
|---|---|---|---|---|---|---|---|---|---|---|---|---|---|---|---|
| | Chl a | | | Chl b | | | Chl c | | | Chl a | | | pheop. | | |
| | I | II | III | I | II | III | I | II | III | I | II | III | I | II | III |
| AL. Swe. | 16 | 7 | 8 | 60 | 20 | 31 | 55 | 14 | 32 | 41 | 11 | 13 | 25 | — | 88 |
| LS. Swe. | 4 | 7 | 6 | 90 | 32 | 17 | 71 | 12 | 50 | 7 | 6 | 5 | 29 | 21 | 24 |
| FBS. Swe. | 6 | 18 | 5 | 27 | 36 | 13 | 47 | 41 | 34 | | | 6 | | | 23 |
| AW. GDR | | | | | | | | | | 27 | 9 | | — | 19 | |
| IMR. Fin. | 4 | 3 | | | | | | | | 5 | 2 | | 17 | 14 | |
| NBW. Fin. | 21 | 33 | | | | | | | | | | | | | |
| IFM. FRG | | 3 | | | 16 | | | 31 | | | | | | | |
| HS I. USSR | | | 7 | | | 22 | | | 32 | | | 27 | | | 108 |
| HS II. USSR | | | 13 | | | 33 | | | 42 | | | 19 | | | 74 |
| Mean | 10 | 12 | 8 | 59 | 26 | 23 | 58 | 25 | 38 | 20 | 7 | 14 | 24 | 18 | 63 |

TABLE 7 A. The relative composition of the phytoplankton biomass at the three intercalibrations.

| Year Date | Algal group | | | | Rel. comp. of the biomass |
|---|---|---|---|---|---|
| | Pyrrophyta | Cyanophyta | Chlorophyta | Chrysophyta | |
| 1974 June 10 | Peridinium spp<br>Rhodomonas spp<br>Dinophysis spp | Aphanizomenon spp | | | 9:1 |
| 1974 June 12 | Peridinium spp<br>Gymnodinium spp<br>Dinophysis spp | Oscillatoria spp | | | 3:2 |
| 1975 July 9 | Amphidinium spp<br>Cryptomonas spp<br>Rhodomonas spp | Oscillatoria spp | Pyramimonas spp | Monades | 3:6:1:2 |

TABLE 7 B. Cholorophylls occurring in the various algal groups. Data given by prof. G. Uherkovich in 1975 in "Syllabus zum algologischen Kurs in Joensuu und Aneboda".

| Algal group | Cholorophyll | | |
|---|---|---|---|
| | a | b | c |
| Cyanophyta | x | | |
| Pyrrophyta | x | | (x) |
| Chlorophyta | x | x | |
| Chrysophyta | x | | (x) |

Merentutkimuslaitos
Lokero 14 166
Helsinki 14

Havsforskningsinstitutet
Fack 14 166
Helsingfors 14

Institute of Marine Research
Box 14 166
Helsinki 14, Finland